Exclusive Electroproduction of Φ Mesons in the ZEUS Experiment

Marcin Sokołowski

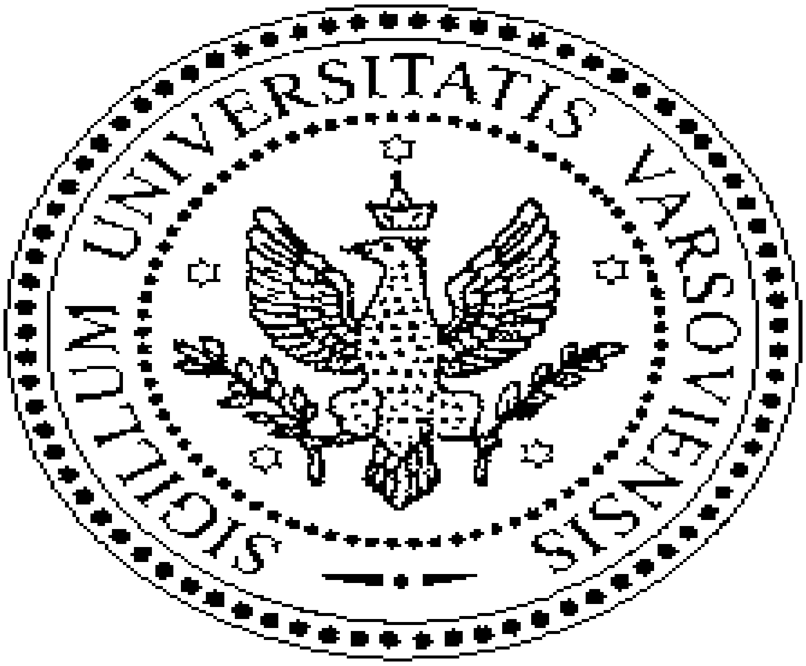

M.Sc. thesis written under supervision of Dr.hab. J. Ciborowski.
Institute of Experimental Physics
Department of Physics
Warsaw University

Warsaw, June, 1998

Abstract

Electroproduction of Φ mesons in $ep \rightarrow ep\Phi$ ($\Phi \rightarrow K^+K^-$) reaction, in the kinematical range 0.25 GeV^2 $< Q^2 <$ 0.85 GeV^2, 25 GeV $< W <$ 90 GeV, $|t| < 0.6$ GeV^2 has been studied using the ZEUS detector. Integrated cross section of $\sigma_{\gamma^* p \rightarrow \phi p}$=$343.0 \pm 25.0(stat.)^{+34}_{-32}(syst.)$ nb for the entire kinematical range has been obtained. The dependence of the cross section on W and Q^2 has also been studied and ratio $R = \sigma_L/\sigma_T$ determined.

Contents

List of Figures

List of Tables

Chapter 1

Introduction

Understanding the structure of the matter has always been one of the main goals of physics. A significant progress in this domain was made by discovery of the electron by Thomson in 1897. In 1911 Rutherford carried out an experiment of scattering α particles on a thin gold foil which led to discovery of the atomic structure.

Further research has led to discovery of the constituents of the nucleus - protons and neutrons and later many other particles. In the 1964 Murray Gell-Mann and George Zweig independently put forward a hypothesis that strongly interacting particles, hadrons, consist of more fundamental objects which they called quarks. Introduction of quarks made possible understanding of the variety of known particles.

Structure of the nucleons (proton, neutron) has been studied in the lepton (electrons, muons ,neutrinos) scattering experiments. Experiments performed in the '70-s in the American centre SLAC (Stanford Linear Acceleration Center) confirmed the hypothesis of the quark structure of hadrons.

In order to obtain higher values of the centre-of-mass energy, construction of the electron-proton collider was proposed. It has been built in the scientific centre DESY (Deutsches Elektronen-SYnchrotron) in Hamburg. The HERA accelerator collides the electron beam of energy up to 30 GeV with the proton beam of energy 820 GeV, reaching centre-of-mass energy $\sqrt{s} \approx 300$ GeV. The main investigations concern :

- diffraction
- photoproduction
- the proton structure functions
- testing Quantum Chromodynamics (QCD)
- *ep* scattering with exchange of charged currents
- search for signals of new hypothetic phenomena beyond the Standard Model (substructure of the quarks and leptons, leptoquarks)

Particular attention is paid to exclusive vector meson production : $ep \to epV^0$ ($V^0 = \rho^0, \omega, \Phi, J/\psi$). It was observed in fixed target experiments [1, 2] that these processes reveal features characteristic of diffraction: weak energy dependence of cross sections, an exponential fall-off of the differential cross section $d\sigma/dt$ (t is the square of the four-momentum transfer at the proton vertex) and conservation of helicity in the s-channel (SCHC). The cross sections for exclusive photoproduction ($Q^2 \approx 0$, where Q^2 is the square of the four-momentum of the virtual photon), of light vector mesons were measured in numerous fixed target experiments [1, 2, 3, 4] and also at HERA [5, 6, 7].

These results are well described in the framework of the Regge theory (soft phenomena) [8] and the Vector Meson Dominance (VMD) model [9]. However both fail to describe

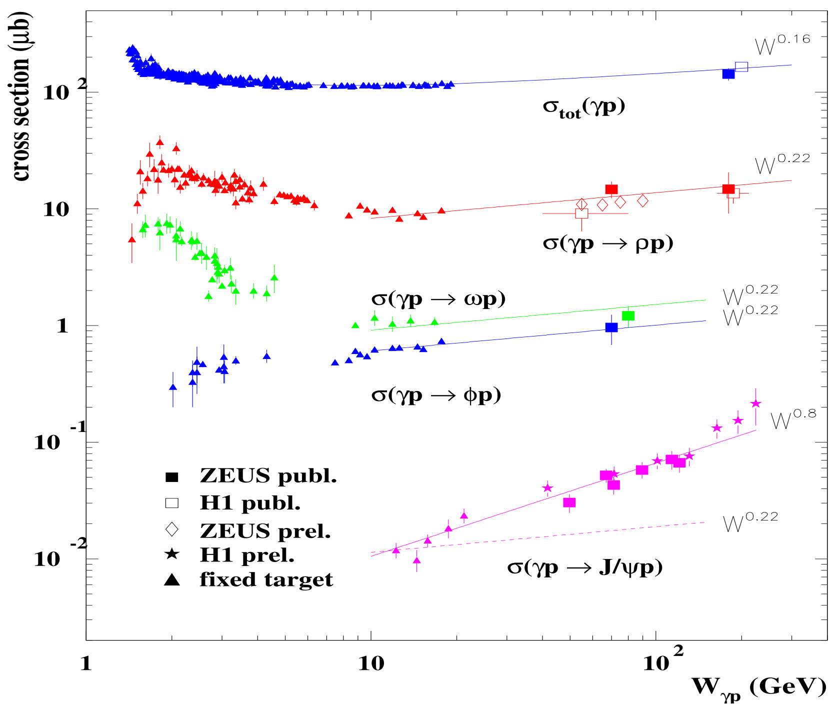

Figure 1.1:

the rapidly raising cross sections for exclusive photoproduction of heavy vector mesons (e.g. J/ψ) [10, 11, 12]. Which is on the other hand well described in the framework of the perturbative QCD (pQCD) [17, 18] (hard phenomena). In the calculations of exclusive J/ψ production, the large scale of the process, which justifies the perturbative approach, is provided by the mass of J/ψ ($M_{J/\psi} \simeq 3.1$ GeV). It is expected that the pQCD may become applicable also to exclusive production of light vector mesons, at sufficiently high values of Q^2 ($Q^2 \gtrsim 20$ GeV^2). The recent measurements of exclusive production cross sections for ρ^0 and Φ in deep inelastic scattering (DIS) for $Q^2 \gtrsim 5$ GeV^2 [13, 14, 15] may be interpreted as an indication that the energy dependence of cross sections may be stronger then in photoproduction (the data cover the Q^2 range up to $Q^2 \sim 27$ GeV^2). The interplay of soft and hard phenomena and the onset of hard phenomena in exclusive vector meson production still remains to be clarified. This task requires measurements of cross sections in a wide range of Q^2. The purpose of this analysis was to measure the cross sections for exclusive Φ production, $ep \rightarrow ep\Phi$, in the low Q^2 region (0.25 GeV^2 $< Q^2 <$ 0.85 GeV^2), which remained unexplored, for the centre-of-mass energies of the photon-proton system 25 GeV $<$ W $<$ 90 GeV. This kinematical region is important because it lies between the photoproduction and DIS. Recent results from exclusive ρ^0 production analysis [16] indicate that the energy dependence of the cross sections in the above region of Q^2 is similar to that measured in photoproduction and is well described by the Regge phenomenology. Because the mass of the Φ meson ($M_\Phi \simeq 1.02$ GeV) is larger then that of ρ^0 ($M_\rho \simeq 0.77$ GeV) it is interesting to compare the behaviour of the cross sections as a function of energy in these two cases.

Another motivation for the present analysis was to investigate a possibility of using particle identification (by means of energy loss, dE/dx) in cross section determination.

This analysis was performed using the data collected with the ZEUS detector in the 1996 running period. Small values of Q^2 became accessible for the physical analysis owning to the installation of the Beam Pipe Calorimeter (BPC) which enables detection of positrons scattered at very small angles (17 mrad $< \theta <$ 35 mrad).

Chapter 2

Electroproduction of Φ mesons

2.1 Kinematics

Fig. 2.1 shows the diagram describing scattering of electrons on protons in the first order of perturbation theory with the exchange of the electroweak gauge boson $(\gamma^*, Z^0, W^\pm)$ [1]. The variables are defined as follows :

k :four-momentum of the incoming positron
k' :four-momentum of the scattered positron
P :four-momentum of the incoming proton
P' :four-momentum of the scattered proton
q=k-k' :four-momentum of the exchanged gauge boson

Using the above notation the following kinematical variables are introduced to describe the *ep* interactions :

- Centre-of-mass energy, $\sqrt{s}$:

  $$s \equiv (k+P)^2 = m_e^2 + m_p^2 + 2(E_e E_p - \vec{p}_e \vec{p}_p) \simeq 4E_e E_p \quad , \tag{2.1}$$

  where E_e and E_p are the positron and proton beam energies respectively. In 1996 these were : E_e=27.5 GeV, E_p=820 GeV, resulting in the centre-of-mass energy of $\sqrt{s} \simeq 300$ GeV.

- The negative four-momentum squared of the virtual photon, Q^2 :

  $$Q^2 \equiv -q^2 = -(k-k')^2 = -2m_e^2 + 2kk' = -2m_e^2 + 2(E_e E_e' - \vec{p}_e \vec{p}_e\,') \quad , \tag{2.2}$$

  where E_e', $\vec{p}_e\,'$ are energy and momentum of the scattered electron.

---

[1] γ^* denotes the virtual photon, beyond the mass threshold ($Q^2 \neq 0$)

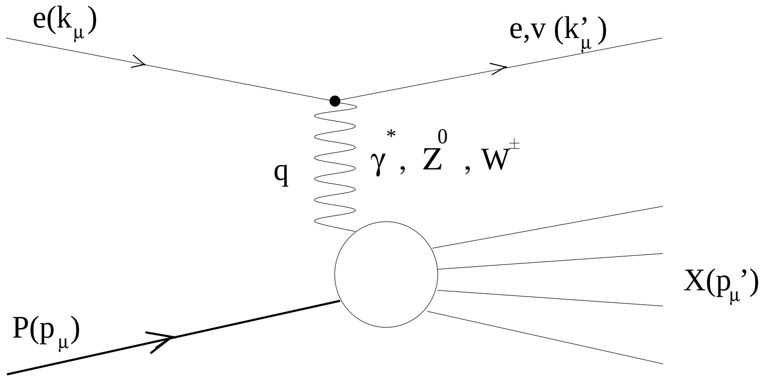

Figure 2.1: *The first order diagram describing process of* $ep \to e\ (\nu)X$ *scattering. For the description of variables - see text.*

- the Bjorken scaling variable, x :

$$x \equiv \frac{Q^2}{2P \cdot q} \quad , \tag{2.3}$$

  which has the interpretation of the fraction of the total momentum of the proton carried by the struck quark (as viewed in the infinite momentum frame).

- the Bjorken variable, y :

$$y \equiv \frac{P \cdot q}{P \cdot k} = \frac{\nu}{\nu_{max}} \quad , \tag{2.4}$$

  where ν is the electron energy transfered to the proton in the proton rest frame and is given by :

$$\nu \equiv (E_e - E_e')_{p\, rest\, frame} = \frac{P \cdot q}{m_p}$$

  and $\nu_{max} \approx s/2m_p$ is the maximal energy that can be transfered to the proton (electron energy in the proton rest frame).

- Energy of the γ^* p centre-of-mass system, W :

$$W^2 \equiv (P+q)^2 = m_p^2 - Q^2 + 2P \cdot q = m_p^2 - Q^2 + ys \quad . \tag{2.5}$$

- four-momentum transfer squared at the proton vertex, t :

$$t \equiv (P - P')^2 \; . \tag{2.6}$$

  Fig. 2.2 shows the diagram of the vector meson production in *ep* interactions with the Pomeron exchange.

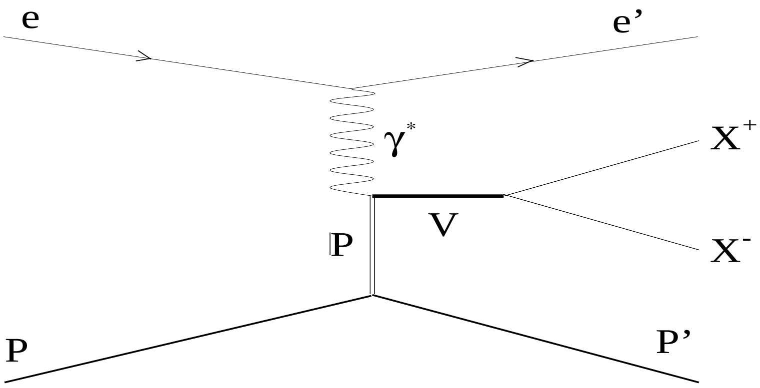

Figure 2.2: *Diagram of the vector meson electroproduction with the Pomeron exchange.*

2.2 Cross Sections

2.2.1 ep cross section

The differential cross section of ep neutral current interaction via the γ^* exchange can be expressed in terms of two structure functions F_1 and F_2 by the following formula [39]:

$$\frac{d\sigma}{dydQ^2} = \frac{4\pi\alpha^2}{Q^4}\left(F_1\left(1-\frac{2m_e^2}{Q^2}\right)xy + F_2\left(\frac{1-y}{y}+\frac{m_p^2 x}{s}\right)\right) \quad , \tag{2.7}$$

where α is the electromagnetic coupling constant. In the quark-parton model (QPM) the structure functions F_1 and F_2 are expressed as :

$$2F_1(x) = \sum_i e_i^2(q_i(x)+\bar{q}_i(x)) \tag{2.8}$$

$$F_2(x) = \sum_i e_i^2 x(q_i(x)+\bar{q}_i(x)), \tag{2.9}$$

where $q_i(x)(\bar{q}_i(x))$ denote the probability of finding a quark(antiquark) of flavour i and charge e_i carrying fraction x of the proton four-momentum and the summation is done over all quark flavours. In this model structure functions depend only on the scaling variable x. The following relation, called Callan-Gross relation holds [44]:

$$2xF_1(x) = F_2(x) \quad . \tag{2.10}$$

2.2.2 γ^*p cross section

The discussion of γ^*p interaction is restricted to the proton rest frame, thus four-momentum of the photon is $q = (\nu, \vec{q})$. The total cross section for scattering real photons (γ) of polarisation ϵ_λ off unpolarised protons was calculated from the Feynman rules to be :

$$\sigma^{tot}(\gamma p \to X) = \frac{4\pi^2\alpha}{K}\epsilon_\lambda^{\mu^*}\epsilon_\lambda^{\nu}W_{\mu\nu} \quad , \tag{2.11}$$

where K is the flux factor. In case of the real photons $K = \nu$ and only transversal polarisations are possible $\lambda = 1, 2$. In order to obtain expression for $\sigma^{tot}(\gamma^* p \to X)$ one requires to know K and ϵ^μ_λ for the case of the virtual photons. The polarisation in this case is assumed to be polarisation of the massive spin 1 particle :

$$\epsilon^\mu_{\pm 1} = \pm \frac{1}{\sqrt{2}}(0, 1, \pm i, 0) \qquad \epsilon^\mu_0 = \pm \frac{1}{\sqrt{Q^2}}(\sqrt{\nu^2 + Q^2}, 0, 0, \nu) \ . \tag{2.12}$$

The most popular choice of the flux factor is based on the convention by Hand [43]. It requires the flux factor K to be equal to the energy of the real photon needed to create an equivalent centre-of-mass energy in the photon-proton CMS. This leads to the following relation :

$$W^2 = \quad m_p^2 + 2m_p K = -Q^2 + 2m_p\nu + m_p^2$$

and yields the following formula for the flux factor of the virtual photons :

$$K_{Hand} = \nu - \frac{Q^2}{2m_p} \ . \tag{2.13}$$

With the above formulae for K_{Hand} and ϵ^ν_λ one obtains the following expressions for the total cross sections for polarised photons:

$$\sigma_T = \frac{1}{2}(\sigma^{tot}_+ + \sigma^{tot}_-) = \frac{4\pi^2\alpha}{Km_p} F_1 \tag{2.14}$$

$$\sigma_L = \sigma^{tot}_0 = \frac{4\pi^2\alpha}{Km_p}\left(\frac{F_2}{2x} - F_1\right) \ . \tag{2.15}$$

After expressing Eq. 2.7 in terms of σ_L and σ_T one obtains the following formula relating the ep differential cross section and $\gamma^* p$ cross sections :

$$\frac{d^2\sigma}{dydQ^2} = \Gamma \cdot (\sigma_T + \epsilon\sigma_L) \ , \tag{2.16}$$

where photon polarisation ϵ and photon flux factor Γ are given by :

$$\epsilon = \frac{2(1-y)}{1 + (1-y)^2} \tag{2.17}$$

$$\Gamma = \frac{\alpha(1 + (1-y)^2)}{2\pi Q^2 y} \ . \tag{2.18}$$

Introducing the ratio $R = \sigma_L/\sigma_T$, Eq. 2.16 can be rewritten in the following form:

$$\frac{d^2\sigma}{dydQ^2} = \Gamma \cdot \sigma_T(1 + \epsilon R) \ . \tag{2.19}$$

In the presented analysis $\sigma_{tot} = \sigma_T + \sigma_L \approx \sigma_T + \epsilon\sigma_L$, since $< \epsilon > \approx 0.999$ in the data.

2.3 Theoretical overview

2.3.1 Vector Meson Dominance Model (VMD)

It was observed that at high energies photon-hadron interactions exhibit similar properties as hadron-hadron. It can be explained by photon fluctuations into a hadronic state with the same quantum numbers, $J^{PC} = 1^{--}$; Q=S=B=C=0, namely a vector meson. Thus the physical photon can be described as a superposition of a bare point-like photon and its hadronic component :

$$|\gamma >= |\gamma >_{bare} + |\gamma >_{hadronic} \quad . \tag{2.20}$$

The lifetime of the fluctuation into the hadronic state of mass M_V is given by [42]:

$$t_f = \frac{2\nu}{Q^2 + M_V^2} \quad . \tag{2.21}$$

Within the framework of the vector dominance model VMD [9] the hadronic component of the photon is assumed to be a superposition of contributions from the lightest vector mesons :

$$|\gamma >_{hadronic} = \sum_{V=\rho^0,\omega,\phi} \frac{M_V^2}{M_V^2 + Q^2} \frac{1}{f_V} |V > \tag{2.22}$$

where f_V is the γV coupling and $|V >$ denotes the wave function of the vector meson V. Using the above ansatz one can determine the following expressions for the total transversal $\sigma^T_{\gamma^* p}(W, Q^2)$ and longitudinal $\sigma^L_{\gamma^* p}(W, Q^2)$ cross sections :

$$\sigma_T^{\gamma^* p}(W, Q^2) = \sum_{V=\rho^0,\omega,\Phi} \frac{4\pi\alpha}{f_V^2} \left(\frac{M_V^2}{M_V^2 + Q^2} \right)^2 \sigma_T^{Vp\to Vp}(W) \tag{2.23}$$

$$\begin{aligned} \sigma_L^{\gamma^* p}(W, Q^2) &= \sum_{V=\rho^0,\omega,\Phi} \frac{4\pi\alpha}{f_V^2} \left(\frac{M_V^2}{M_V^2 + Q^2} \right)^2 \frac{Q^2}{M_V^2} \sigma_L^{Vp\to Vp}(W) \\ &= \sum_{V=\rho^0,\omega,\Phi} \frac{4\pi\alpha}{f_V^2} \left(\frac{M_V^2}{M_V^2 + Q^2} \right)^2 \frac{Q^2}{M_V^2} \xi^2 \sigma_T^{Vp\to Vp}(W) \quad , \end{aligned} \tag{2.24}$$

where $\sigma_L^{Vp\to Vp}$, $\sigma_T^{Vp\to Vp}$ are elastic $Vp \to Vp$ longitudinal and transverse cross sections, $\xi = \sigma_L^{Vp\to Vp} / \sigma_T^{Vp\to Vp}$.

Elastic Φ electroproduction cross section

The VMD relates the $\gamma p \to \Phi p$ to elastic $Vp \to Vp$ cross section as follows:

$$\sigma^{\gamma p\to Vp}(W) = \frac{4\pi\alpha}{f_V^2} \sigma^{Vp\to Vp}(W) \quad . \tag{2.25}$$

Using the above relation together with the Eq. 2.23 and 2.24 reduced to the Φ production case one obtains :

$$\sigma_T^{\gamma^* p \to \Phi p}(W, Q^2) = \left(\frac{M_\Phi^2}{M_\Phi^2 + Q^2} \right)^2 \sigma_T^{\gamma^* p \to \Phi p}(W) \tag{2.26}$$

$$\sigma_L^{\gamma^* p \to \Phi p}(W, Q^2) = \left(\frac{M_\Phi^2}{M_\Phi^2 + Q^2} \right)^2 \xi^2 \frac{Q^2}{M_\Phi^2} \sigma_T^{\gamma^* p \to \Phi p}(W) \ . \tag{2.27}$$

From the above formulae it follows that within the VMD-model the previously defined ratio $R = \xi^2 \cdot Q^2/M_\Phi^2$. After substituting the above formulae into Eq. 2.16 the following formula is obtained :

$$\frac{d^2\sigma^{ep \to ep\Phi}}{dydQ^2} = \phi(y, Q^2) \cdot \sigma_T^{\gamma p \to \Phi p}(W) \ , \tag{2.28}$$

where $\phi(y, Q^2)$ is the effective photon flux :

$$\phi(y, Q^2) = \frac{\alpha}{2\pi} \frac{1}{Q^2} \left(\frac{1 + (1-y)^2}{y} + \frac{2(1-y)}{y} \xi^2 \frac{Q^2}{M_\Phi^2} \right) \left(\frac{M_\Phi^2}{M_\Phi^2 + Q^2} \right)^2 \ . \tag{2.29}$$

Using the Eq. 2.17 and 2.18 one can express the *ep* cross section in the following form :

$$\frac{d^2\sigma^{ep \to ep\Phi}}{dydQ^2} = \Gamma(1 + \epsilon R) \left(\frac{M_\Phi^2}{M_\Phi^2 + Q^2} \right)^2 \sigma_T^{\gamma^* p \to \Phi^0 p}(W) \ . \tag{2.30}$$

2.3.2 Regge phenomenology

Long before formulation of QCD as a theory of strong interactions one of the most successive approaches were phenomenological models. Regge's idea of scattering amplitudes analytically continued in the complex momentum plane is the one which allows to estimate the characteristic features of the hadronic interactions behaviour in the high energy limit. Even now when the QCD is a well defined theory it is still very useful as perturbative QCD calculations are successful only at high energy scales. A detailed discussion of the Regge theory can be found elsewhere [8]. In this approach the t dependence of the differential cross section reads :

$$\frac{d\sigma}{d|t|} \propto e^{-b_0|t|} \left(\frac{W^2}{W_0^2} \right)^{2(\alpha(t)-1)} , \tag{2.31}$$

where $\alpha(t) = \alpha(0) + \alpha' t$ is the Pomeron trajectory and W_0 is energy scale factor which was determined empirically to be comparable to the hadronic mass scale of 1 GeV [20, 21]. Fits to hadron-hadron and photoproduction data give $\alpha(0) = 1.085$ and $\alpha' = 0.25$ GeV^{-2} [22]. The cross section $d\sigma/dt$ can be rewritten in the form :

$$\frac{d\sigma}{d|t|} \propto e^{-b|t|}, \tag{2.32}$$

where b=$b_0+2\alpha' ln\frac{W^2}{W_0^2}$. The W dependence of the cross section can obtained from Eq. 2.31 by integrating over t :

$$\sigma(W) \propto \frac{1}{b_0 + 2\alpha' ln\frac{W^2}{W_0^2}} \cdot \left(\frac{W}{W_0}\right)^{2(\alpha(0)-2)} \propto W^{0.22} \quad . \tag{2.33}$$

In the case of light vector meson electroproduction, the above formula gives a good description of the W dependence of the cross sections in the small Q^2 region (Fig. 1.1).

2.3.3 Perturbative QCD Models for Vector Meson Production

The perturbative approach is justified when the energy scale, $\bar{q}^2$, involved in the process is large (i.e. $\alpha_s(\bar{q}^2)$ is small). The choice of the scale differs in various QCD models, e.g. in the model of Ryskin et al. [17] it is defined as :

$$\bar{q}^2 = \frac{M_V^2 + Q^2 + |t|}{2} \quad . \tag{2.34}$$

In the case of the J/ψ electroproduction the hard scale is provided by its large mass ($M_{J/\psi} \simeq 3.1$ GeV). It is expected that the pQCD models should also describe the electroproduction of light vector mesons at higher values of Q^2 ($Q^2 \gtrsim 20$ GeV^2). The pQCD models predict a strong energy dependence of the cross sections, typically $\sigma(W) \propto W^{0.8-1.6}$.

2.3.4 Angular distributions

An important question is whether the helicity of the virtual photon is retained by the vector meson in the s-channel $\gamma^* p \to \Phi p$ (s-channel helicity conservation-SCHC). Analysis of angular distributions of the Φ meson decay products gives a possibility of testing SCHC hypothesis and determination of the ratio R=σ_L/σ_T. Fig. 2.3 shows the definitions of the angles used in the analysis. The angles are defined in the Φ meson rest frame where the axes are defined as follows : $\vec{x} - \vec{z}$ plane is the production plane, $\vec{y}$ is normal to this plane and $\vec{z}$ axis is opposite to the outgoing proton direction. In this frame the θ_h angle is defined as the angle between the momentum vector of the positive kaon from the Φ meson decay and the $\vec{z}$ axis, ϕ_h is the angle between the decay plane and the production plane and Φ_h is the angle between the electron scattering plane and the production plane. The general form of the angular distribution is given by the following formula [41]:

$$\begin{aligned} & W(\cos\theta_h, \phi_h, \Phi_h) = \\ & \qquad \frac{3}{4\pi}[\frac{1}{2}(1 - r_{00}^{04}) + \frac{1}{2}(3r_{00}^{04} - 1)\cos^2\theta_h \\ & - \quad \sqrt{2}Re(r_{10}^{04})\sin 2\theta_h \cos\phi_h - r_{1-1}^{04}\sin^2\theta_h \cos 2\phi_h \end{aligned}$$

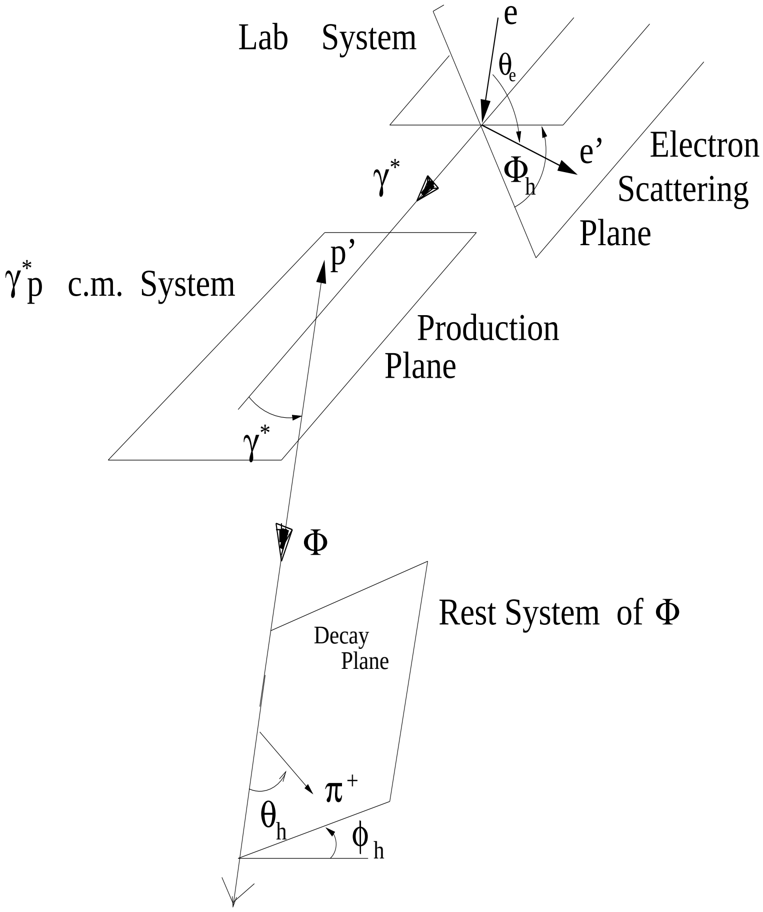

Figure 2.3: The Φ decay angles in the s-channel helicity system.

$$\begin{aligned}
&- \quad \epsilon \cos 2\Phi_h \left(r^1_{11} \sin^2\theta_h + r^1_{00} \cos^2\theta_h - \sqrt{2} Re(r^1_{10}) \sin 2\theta_h \cos\phi_h - r^1_{1-1} \sin^2\theta_h \cos 2\phi_h \right) \\
&- \quad \epsilon \sin 2\Phi_h \left(\sqrt{2} Im(r^2_{10}) \sin 2\theta_h \sin\phi_h + Im(r^2_{1-1}) \sin^2\theta_h \sin 2\phi_h \right) \\
&+ \quad \sqrt{2\epsilon(1+\epsilon)} \cos\Phi_h \{ r^5_{11} \sin^2\theta_h + r^5_{00} \cos^2\theta_h - \sqrt{2} Re(r^5_{10}) \sin 2\theta_h \cos\phi_h \\
&- \quad r^5_{1-1} \sin^2\theta_h \cos 2\phi_h \} \\
&+ \quad \sqrt{2\epsilon(1+\epsilon)} \sin\Phi_h \{ \sqrt{2} Im(r^6_{10}) \sin 2\theta_h \sin\phi_h + Im(r^6_{1-1}) \sin^2\theta_h \sin 2\phi_h \}] \ , \qquad (2.35)
\end{aligned}$$

where ϵ is given by Eq. 2.17 and the r^α_{ij} are parameters related to the spin density matrix elements. Assuming the SCHC only r^{04}_{00}, r^1_{1-1}, $Im(r^2_{1-1})$, $Re(r^5_{10})$ and $Im(r^6_{10})$ may be different from zero and additionally the following relations hold :

$$Im(r^6_{1-1}) = -r^1_{1-1} \qquad Im(r^6_{10}) = -Re(r^5_{10}) \ .$$

If in addition one assumes the natural parity exchange in the t channel ($P = (-1)^J$) Eq. 2.35 reduces to :

$$\begin{aligned}
W(\cos\theta_h, \psi_h) \quad = \quad & \frac{1}{1+R\epsilon} \cdot \frac{3}{8\pi} [\sin^2\theta_h (1 + \epsilon \cos 2\psi_h) + 2\epsilon R \cos^2\theta_h \\
- \quad & \sqrt{2\epsilon(1+\epsilon)R} \cos\delta \sin 2\theta_h \cos\psi_h] \ , \qquad (2.36)
\end{aligned}$$

where $\psi_h = \Phi_h - \phi_h$ and δ is the relative phase between the two helicity amplitudes. Several matrix elements can be determined from distributions of $\cos\theta_h, \phi_h, \psi_h$ which can be obtained by integrating Eq. 2.36 :

$$\frac{1}{N}\frac{dN}{d\cos\theta_h} = \int_0^{2\pi} d\psi_h W(\cos\theta_h, \psi_h) = \frac{3}{4}\left[1 - r_{00}^{04} + \left(3r_{00}^{04} - 1\right)\cos^2\theta_h\right] \tag{2.37}$$

$$\frac{1}{N}\frac{dN}{d\psi_h} = \int_{-1}^{1} d(\cos\theta_h) W(\cos\theta_h, \psi_h) = \frac{1}{2\pi}\left(1 + 2\epsilon r_{1-1}^{1}\cos 2\psi_h\right) \quad . \tag{2.38}$$

Thus matrix elements r_{00}^{04}, r_{1-1}^{1} can be determined by fitting Eq. 2.37 and 2.38 to experimental distributions of $\cos\theta_h$ and ψ_h. Assuming SCHC, the ratio R is given by the formula :

$$R = \frac{1}{\epsilon} \cdot \frac{r_{00}^{04}}{1 - r_{00}^{04}} \ . \tag{2.39}$$

Chapter 3

The ZEUS detector and HERA

3.1 HERA collider

The Hadron-Elektron-Ring-Anlage 'HERA' is designed to collide 820 GeV protons and 30 GeV positrons. The HERA machine was build in the years 1984-90 in cooperation of institutes from 12 countries.

The storage rings of circumference of 6.3 km are placed in the tunnel 10-25 m underground. In order to keep protons on their orbits super-conducting magnets of 4.6 T were used and this limits maximal proton energies that can be achieved at HERA. In case of positrons conventional magnets are sufficient, limitation of positron energy is due to energy dissipations coming from synchrotron radiation. The overview of HERA accelerating complex is shown on Fig. 3.1. In spite of the fact that the design values of performance has not been achieved, they has been improved year by year. Much effort was put into increasing luminosities from approximately 30 nb^{-1} in 1992 up to 32 pb^{-1} in 1997 (Tab. 3.1). Two oppositely circulating beams collide in two experimental halls where ZEUS and H1

Figure 3.1: *Overview of HERA collider and HERA pre-accelerating complex.*

Parameter	Design value	1992	1994	1996
proton energy E_p(GeV)	820	820	820	820
positron (energy) E_e(GeV)	30	26.7	27.5	27.5
centre of mass energy $\sqrt{S}$(GeV)	314	296	300	300
Integrated luminosity $L_{int}(pb^{-1})$	100	0.05	6.2	10.6

Table 3.1: *Overview of HERA performance.*

detectors are installed. The other two HERA experiments HERMES and HERA-B are stationary target experiments and make use of positron and proton beams respectively. The HERMES experiment takes advantage of longitudinal polarisation of the positron beam in order to investigate spin structure of nucleons. In the HERA-B experiment is currently under installation, it will use the proton beam only.

3.2 The ZEUS Detector

The ZEUS detector has been extensively described in a number of publications [53]. The ZEUS multi-purpose detector was build and operated by the collaboration of 450 physicists from 50 institutes of 12 countries. The detector is located 30 meters underground in the South Hall, it is $10 \times 15m^2$, 11 m high and its mass is about 3600 tons. Fig. 3.2 shows the geometry of the ZEUS detector, it is described by right handed Cartesian coordinate system with its origin in the interaction point (IP). The Z axis is pointing along the direction of the incoming proton, the X axis is also horizontal and points towards the centre of the HERA ring. The direction of Y axis is determined by ZX-axis and points vertically in upper direction. The polar angle θ is measured with respect to Z-direction and ϕ is the azimuthal angle with respect to X axis. Thus, the polar angle of proton and positron beam is equal to $0°$ and $180°$ respectively. Components most relevant for this analysis will now be described.

3.2.1 Uranium Calorimeter (UCAL)

The ZEUS sampling calorimeter is constructed as a sandwich of depleted uranium and scintillator tiles. Particles incidenting on the calorimeter shower with charged particles which induce a light response in the scintillators. Light pulses from individual scintillators are transfered through wavelength shifters and readout in photomultiplier tubes.

The ZEUS calorimeter is divided into three major sections FCAL,BCAL,RCAL [1] which cover the following ranges of polar angles : $2.2° < \theta < 39.9°$, $36.7° < \theta < 129.1°$, $12.1° < \theta < 176.5°$ respectively. Each section is subdivided transversally into minor sec-

---

[1] F-forward,B-barrel,R-rear

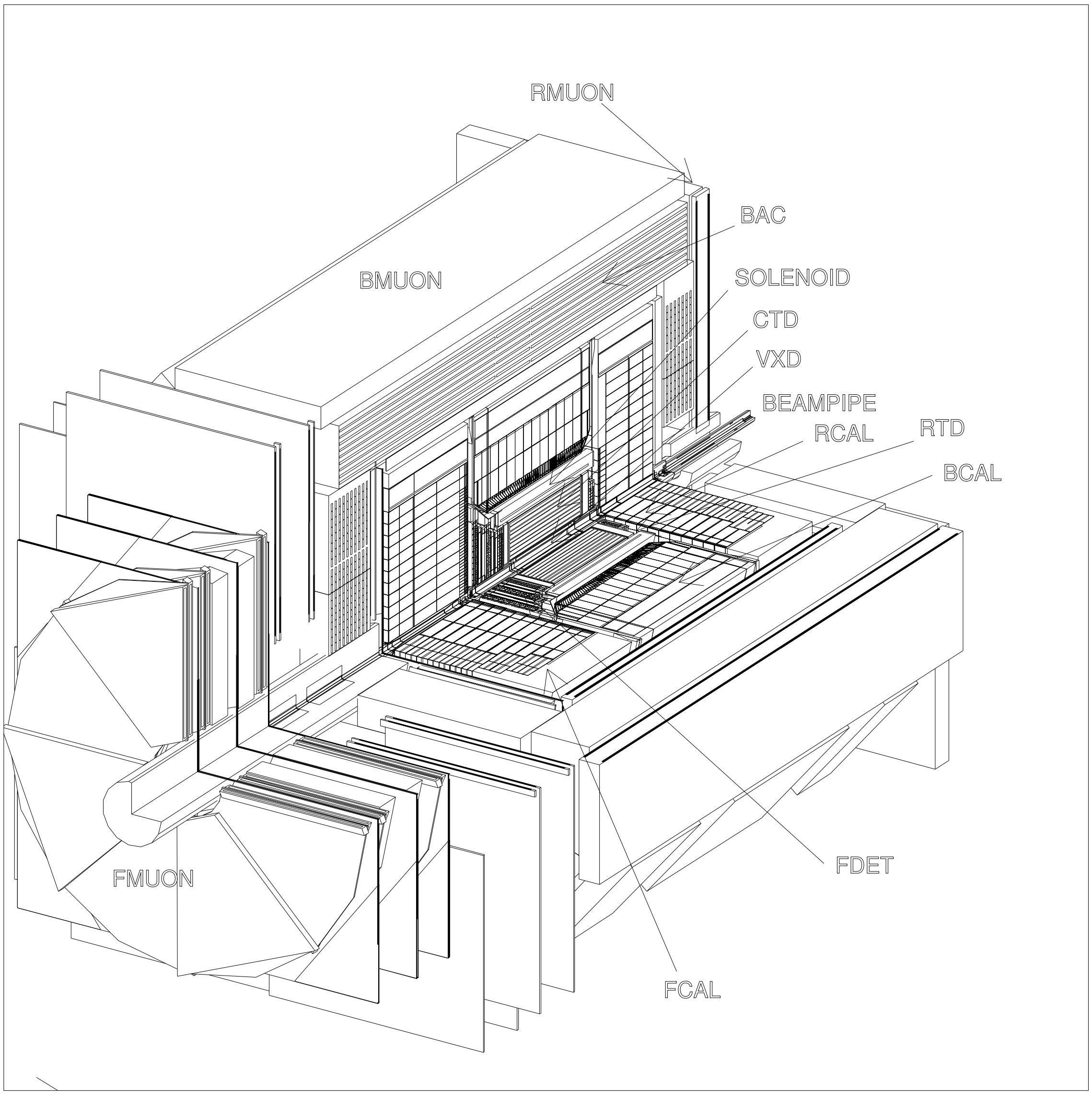

Figure 3.2: *Overview of ZEUS detector.*

tions called *towers* which consist of smaller entities called *cells*. Each part has 2 longitudinal sections, electromagnetic (EMC) and hadronic (HAC). Thickness of the uranium and scintillator tiles were tuned to give identical responses for electron and hadrons of the same energy (compensation). In order to fully contain electromagnetic and hadronic showers, EMC sections have a depth of $\propto$ 25 radiation lengths X_0 while HAC sections depth vary from $3\lambda_0$ in RCAL to $6\lambda_0$ in FCAL. Energy resolution in UCAL was determined under the beam test conditions to be:

$$\frac{\sigma_E^{EMC}}{E} = \frac{0.18}{\sqrt{E}} \oplus 0.01 \qquad\qquad \frac{\sigma_E^{HAC}}{E} = \frac{0.35}{\sqrt{E}} \oplus 0.02 \ .$$

Good time resolution [2] of individual cell was achieved to be : $\Delta t \simeq 1$ ns, for energy

---

[2] Comparing to the time between bunch crossings, 96 ns.

deposits $\geq$ 4.5 GeV and is used to reject background beam-gas and cosmic events.

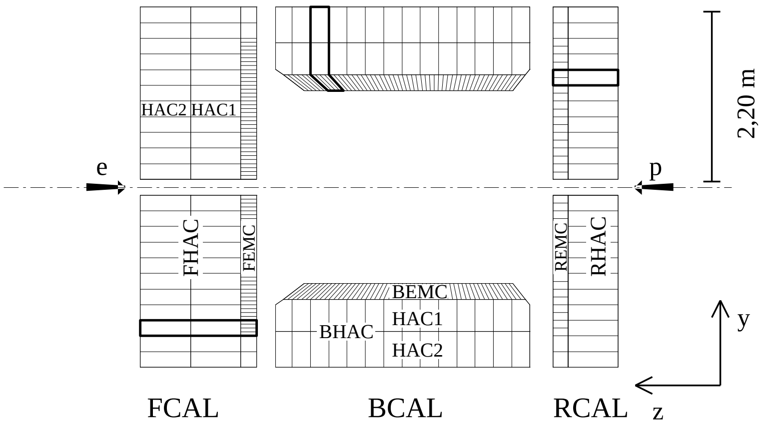

Figure 3.3: *Uranium calorimeters with EMC and HAC sections visible.*

3.2.2 Central Tracking Detector (CTD)

Central Tracking Detector is a cylindrical drift chamber with a length 240 cm, inner and outer diameters of 32.4 and 164.8 cm respectively. This corresponds to angular coverage in polar angle of $15^\circ < \theta < 164^\circ$. The chamber is filled with a gas mixture of Ar : CO_2 : C_2H_6 (90:8:2). The CTD consists of 4608 wires which are organised in 72 cylindrical drift layers, divided in 9 superlayers (Fig. 3.4). Wires from odd numbered superlayers are parallel to Z axis while wires from even numbered superlayers have an angle tilts between -5.53 and +5.62 to provide a stereo view. This allows to measure $r\Phi$ position with a resolution of 100-120 μm . The Z position is measured by z-timing system, layer 1 and alternate wires from layers 3 and 5 are equipated with fast readout system that makes possible measuring arrival times of the signal at both ends of a single wire, resolution of this method is $\sigma_z \lesssim 3cm$. In order to measure the momentum of the particles CTD is surrounded by a solenoid which provides a magnetic field of 1.43 T. The momentum resolution of the CTD was measured to be : $\sigma_{p_t}/p_t = \sqrt{(0.005 \cdot p_t)^2 + (0.016)^2}$, where p_t is the transverse momentum of particle in the LAB frame measured in GeV. The digitised pulse height from CTD wire is proportional to energy lost by charged particle for ionising the gas medium, this enables to determine with a good accuracy the dE/dx.

3.2.3 Beam Pipe Calorimeter (BPC)

The BPC is an electromagnetic sampling calorimeter consisting of two modules, BPC-North and BPC-South,which are placed on both sides of the beampipe 294 cm from the interaction point in the rear direction. The BPC calorimeter consists of 26 tungsten plates each about 130 mm×130 mm and 3.5 mm thick, separated by 2.6 mm thick scintillator

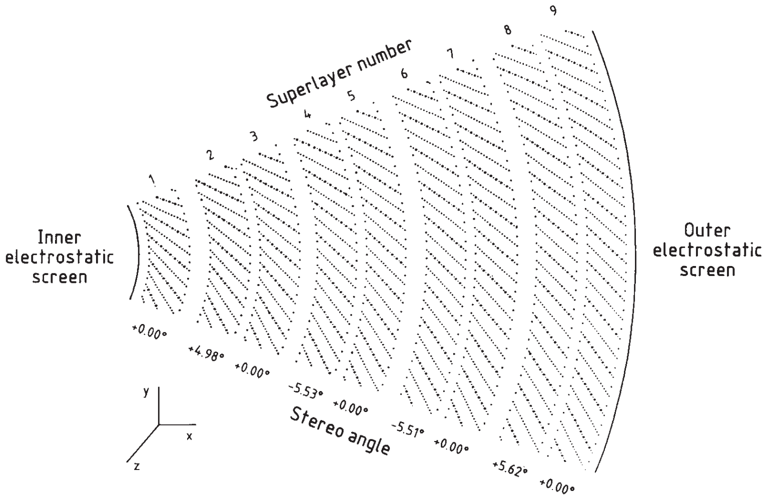

Figure 3.4: *Arrangement of wires in one octant of the CTD.*

layers. Thus the longitudinal size of the single module is about 16 cm corresponding to 26 radiation lengths X_0. Scintillator layers are divided into strips of width 8 mm and alternate scintillator layers have strips perpendicular providing XY position information.

The main goal of installing the BPC detector (1995) was to extend the kinematical coverage of the ZEUS detector. The angular acceptance of the BPC is 17 mrad$< \theta <$35 mrad which allows to access the following region of kinematical variables $0.1 < Q^2 < 0.9$ and $10^{-6} < x < 10^{-4}$. In the present analysis only BPC-North module has been used, in which fiducial area of 4.8 cm × 6.0 cm define high acceptance and good resolution region. Because the fiducial area is very small, the BPC allows to cover only a small part of the solid angle ($\approx$ 13%) corresponding to the accessible region of kinematical variables Q^2, x. Energy resolution of BPC calorimeter was measured under beam test conditions to be : $\sigma_E/E = 0.17/\sqrt{E}$. Overview of the BPC setup is presented on Fig. 3.5. A detailed description of the BPC calorimeter can be found elsewhere [34].

3.2.4 Proton Remnant Tagger (PRT)

PRT is a system of seven pairs of scintillators situated at 5.15 m (PRT1) and 24m (PRT2) from the IP in the forward direction. Fig. 3.6 shows location of PRT stations and their geometrical acceptance. The PRT allows registering particles moving at very small angles with respect to the incoming proton direction.

3.2.5 Luminosity Monitor

The luminosity is a measure of the machine performance, it can be defined as follows :

$$L = \frac{I_p I_e}{4\pi e^2 f B \sigma_x \sigma_y} \tag{3.1}$$

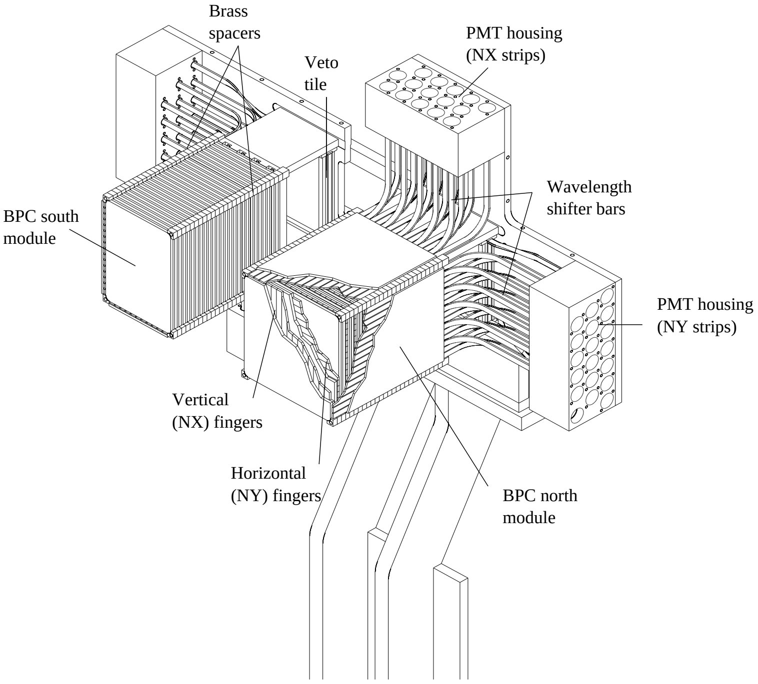

Figure 3.5: *BPC setup.*

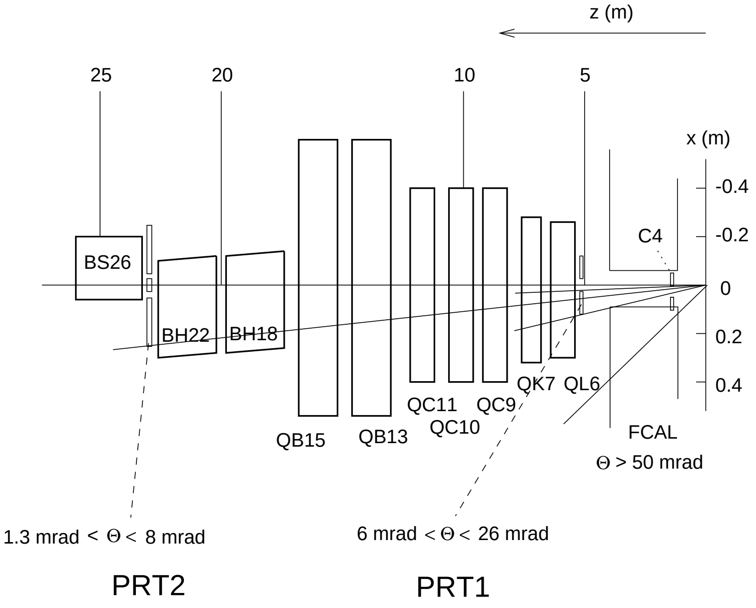

Figure 3.6: *PRT location.*

where I_p, I_e are proton and electron currents , f frequency of bunch crossings, B number of the circulating bunches and σ_x, σ_y are horizontal and vertical extensions of a bunch. For the purpose of physical analysis a relevant quantity is an integrated luminosity $L_{int} = \int L dt$, where integration is performed over the time of the data collection. Cross section σ_{proc} for a given kinematical process can be determined form the following formula :

$$\sigma_{proc} = N_{proc}/L_{int} \ , \tag{3.2}$$

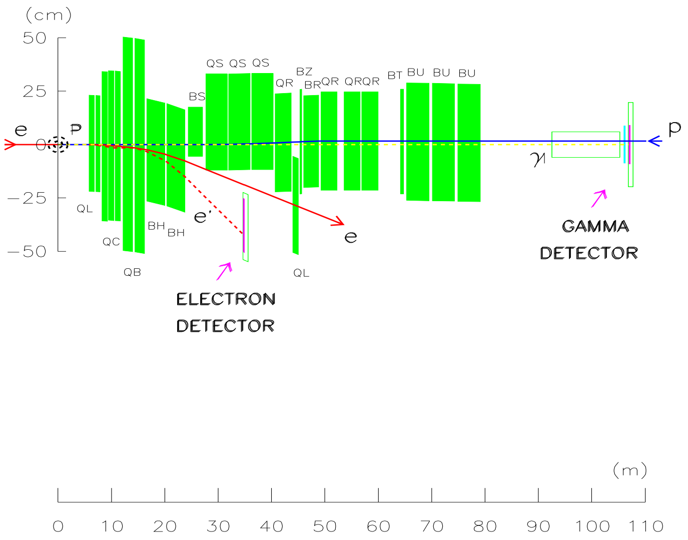

Figure 3.7: *Setup of the luminosity monitoring system.*

where N_{proc} is the total number of events which occured during the data collecting period. The usual way of measuring luminosity is counting number of events of physical process of a well known cross section. In the ZEUS experiment it is measured by counting number of $ep \to ep\gamma$ events. Because this is a QED process its cross section is known with a good precision and is described by Bethe-Heitler formula [61]. The luminosity monitor is a system of 2 calorimeters that tag photons and electrons scattered in Bethe-Heitler process. Photons emitted in $ep \to ep\gamma$ process can propagate in the proton pipe and leave it 80 m from the IP after a bend of the proton beam, while slightly off-beam energy electron is deflected out of the beam pipe by the electron beam magnet BH04 and can be registered by lumi-electron calorimeter (Fig. 3.7). The rate of coincidences between the two calorimeters determines the physics delivered luminosity of the ZEUS experiment.

3.2.6 Trigger system

Because the frequency of bunch crossings is high ($\approx$ 10 MHz) the data in ZEUS detector has to be preselected on-line in order to reduce the stream of data that has to be stored on disks. The ZEUS data acquisition and trigger system has to reduce the data stream from 5 Tbytes/s to about 1 Mbytes/s. High rate of events is mainly due to events which are not ep interactions. The dominant sources of non *ep* background are interactions of the proton and electron beam with the residual gas, beam halo interactions, cosmic ray events. The reduction of data stream is achieved by rejection of events which are likely to be background processes without loosing to many *ep* events. The ZEUS trigger is organised as a three level decision. First two steps (FLT and SLT) are local to single component and the global decision is undertaken by GlobalFLT(GSLT) which combines decisions from subcomponents. To trigger elastic vector mesons production with the positron in BPC a dedicated trigger was developed and will this be described in Sec. 4.2.

- First Level Trigger (FLT)
  uses raw information like energy sums, activity in CTD, timings from few components (CAL,CTD,VETOWALL). At the FLT level only events classified to at least one of the several brunches of physical processes are accepted. The reduction factor of FLT is 10^4 so event rate at SLT is about 500 Hz.

- Second Level Trigger (SLT)
  uses information from VETOWALL,BCAL to reject background events by timing constraints. The reduction factor is about 5, the output rate of SLT is low enough ($\simeq$ 100Hz) to perform reconstruction alghoritm (event builder) similar to the off-line one and make selection with more precise information. The event builder alghoritm combines and formats all data from components into one data set so called *event*.

- Third Level Trigger (TLT)
  At this stage events are analysed more precisely, mainly information from CAL (in case of this analysis also BPC) and CTD is used. Events are classified among several brunches of physical processes, marked with DST bit and written to the disks.

Chapter 4

Reconstruction and Selection of Exclusive Φ events

4.1 Off-line Reconstruction of Events

Reconstruction of exclusive Φ meson production events uses information from the CTD and the BPC.

4.1.1 Track and Vertex Reconstruction in the CTD

The package VCTRAK [55] is the tool for the spatial reconstruction of tracks and vertices in the CTD. The reconstructed tracks enable determination of vertex position, momenta, charges and energy loss dE/dx of particles. In this analysis only events with two tracks in the CTD are considered, as the scattered electron does not enter the acceptance region of the CTD. A typical event is shown on Fig. 4.2.

The number of exclusive $\Phi \rightarrow K^+K^-$ production events in the sample is determined from the invariant mass distribution, M_{KK} which is defined as :

$$M_{KK} = \sqrt{(E_1 + E_2)^2 - (\vec{p}_1 + \vec{p}_2)^2}, \tag{4.1}$$

where $\vec{p}_i$ denote the momenta of the tracks and $E_i = \sqrt{\vec{p}_i^{\,2} + m_K^2}$ denote their energies with the charged kaon mass (m_K=0.49368 GeV) assumed.

4.1.2 Reconstruction of kinematics

In order to reconstruct kinematical variables Q^2, W and t the so called **constrained** method [54] has been used. Let us define the following variable:

$$\delta \equiv E - p_z = \sum_{i,particles} (E - p_z)_i. \tag{4.2}$$

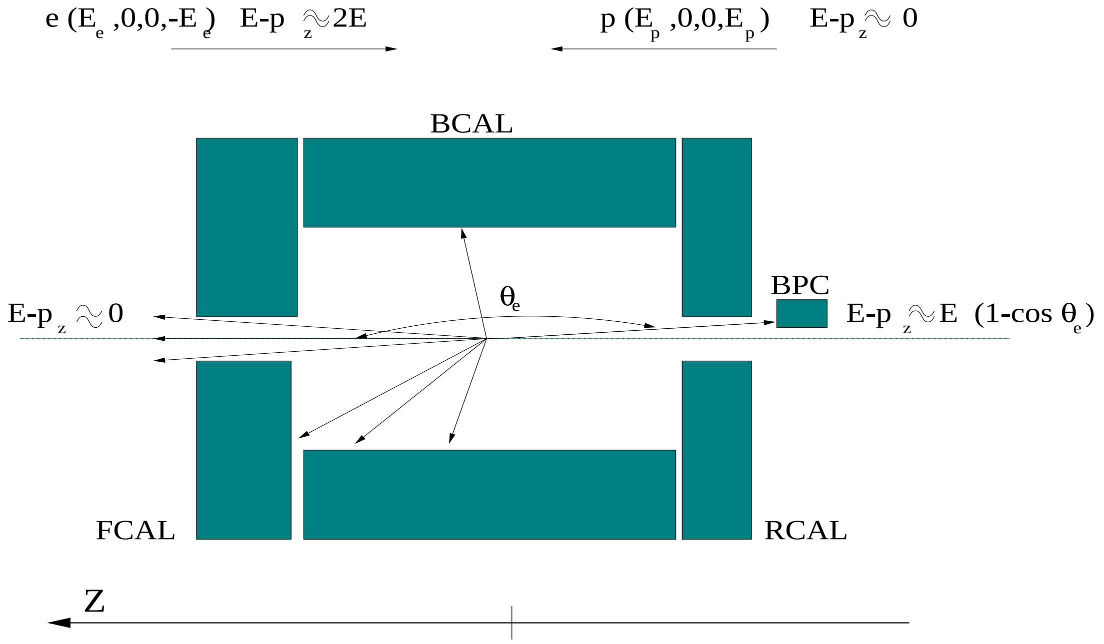

Figure 4.1: *$E - p_z$ conservation. Before interaction, $E - p_z \simeq 2E_e$. After interaction, particles which leave detector through FCAL beampipe carry little $E - p_z$, which can be neglected. The total $E - p_z$ is always conserved .*

Because both energy E and longitudinal momentum p_z are conserved in the interaction, $(E - p_z)$ is also conserved (Fig. 4.1) :

$$(E - p_z)_{initial} = (E - p_z)_{final} . \tag{4.3}$$

As described in Sec. 3.2, in the ZEUS experiment the Z axis is directed along the momentum of the incoming proton, therefore, neglecting the proton mass : $\delta_{proton} = (E - p_z)_{proton} \simeq 0$. The incoming electron moves in the opposite direction and its longitudinal momentum is approximately equal to its negative energy, thus $\delta_{electron} = (E - p_z)_{electron} \simeq 2E_e$. As a result one obtains : $\delta_{initial} \simeq 2E_e$. Assuming the event to be due to exclusive Φ electroproduction, δ after the interaction can be written as :

$$\delta_{final} = (E - p_z)_{p\prime} + (E - p_z)_{electron} + (E - p_z)_{\Phi}. \tag{4.4}$$

Because the scattered proton ($p\prime$) escapes down the beam pipe, the maximal possible value of $\delta_{p\prime} \simeq E_{p\prime}(1 - cos(2.2\,\mathrm{deg})) \simeq 0.0006E_{p\prime}$. Thus the first term in the Eq. 4.4 can be neglected and the Eq. 4.4 can be rewritten as :

$$\delta_{final} = E'_e(1 - cos\theta_e) + (E - p_z)_{\Phi}, \tag{4.5}$$

where the angle θ_e is the scattering angle of the electron with respect to the Z axis and is measured in the BPC.

Conservation of the quantity $(E - p_z)$ in the interaction implies the following relation:

$$2E_e = E'_e(1 - cos\theta_e) + (E - p_z)_{\Phi}, \tag{4.6}$$

from which the energy of the scattered electron can be evaluated:

$$E'_e = \frac{2E_e - (E_\Phi - p_{z,\Phi})}{1 - cos\theta_e}. \tag{4.7}$$

Using Eq. 2.2, 2.4 and 2.5 one may determine the kinematical variables Q^2, y and W :

$$Q^2 = 4E_e E'_e \cos^2 \frac{\theta_e}{2} \tag{4.8}$$

$$y = 1 - \frac{E'_e}{2E_e}(1 - cos\theta_e) \tag{4.9}$$

$$W \simeq \sqrt{ys}. \tag{4.10}$$

The four-momentum transfer t (Eq. 2.6) can be expressed in terms of the measured variables as :

$$t = (P_\Phi - q)^2 \simeq -\left[(p\prime_{e,x} + p_{\Phi,x})^2 + (p\prime_{e,y} + p_{\Phi,y})^2\right] \ . \tag{4.11}$$

4.2 Selection of exclusive Φ production events

The present analysis is based on the data collected in 1996 consisting of runs from 20718 to 22954, except runs 22072-22226 in which an unexpected increase of noise in the BPC was observed. The total amount of data used in this analysis corresponds to the integral luminosity $L_{int} = 9.79\ pb^{-1}$. In order to select events of exclusive Φ production, $ep \to ep\Phi$, with the subsequent decay $\Phi \to K^+K^-$, the following on-line and off-line selections were applied.

4.2.1 On-line selection (trigger)

The requirements at the trigger level were as follows :

1. first level (FLT): (i) energy in BPC $E_{BPC} > 0$; (ii) at least one good track candidate in the CTD (FLT bit 32).

2. second level (SLT): (i) number of tracks in the CTD less then 4; (ii) BPC fiducial cuts (see below); (iii) Z coordinate of the vertex -60 cm $< Z_{vtx} <$ 60 cm or in case of no reconstructed vertex, number of unmatched track segments less then 15.

3. third level (TLT): (i) only one reconstructed vertex and two tracks in the CTD; (ii) Z coordinate of the vertex -66 cm $< Z_{vtx} <$ 66 cm (TLT bit 23).

Events accepted by the above criteria were marked with the DST bit 55 and written to a disk in the MINIDST format.

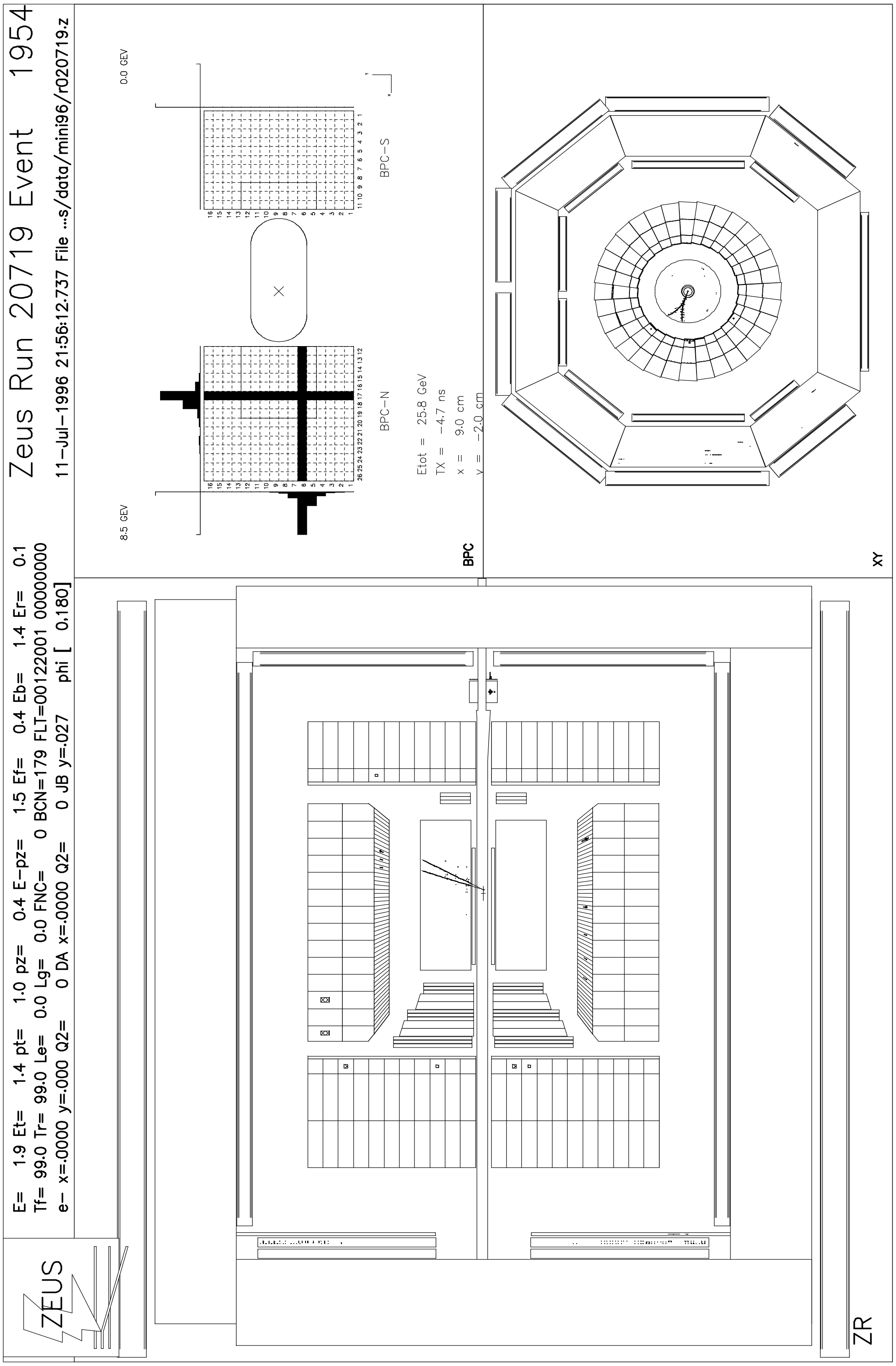

Figure 4.2: *An exclusive BPC Φ electroproduction event displayed with the program LAZE. Position of scattered positron is determined in the BPC and kaon tracks are reconstructed in the CTD.*

4.2.2 Off-line data selection

The following requirements were imposed off-line:

1. Invariant mass cut: $M_{KK} < 1.2$ GeV

2. BPC energy cut : the energy deposited by the positron in the BPC, $E_{BPC} > 20$ GeV.

3. BPC timing cut : the BPC timing is required to be within 3 ns of the time for the e^+p collision: $|t_{BPC} - < t_{BPC} > | < 3$ ns, where $< t_{BPC} > \simeq -5$ ns denotes the average BPC timing.

4. BPC fiducial cuts : only events with the positron position (X,Y) in the BPC in the following range (fiducial volume) were accepted :

   $$[5.17 \text{ cm} < X < 9.97 \text{ cm}] \text{ AND } [-2.82 \text{ cm} < Y < 3.18 \text{ cm}]$$

   This condition allows to accept only those events which have well reconstructed kinematical variables.

5. The shower width was required to be [1] : $\sigma_X < 0.7$ AND $\sigma_Y < 0.7$

6. Vertex position cut:

   The Z coordinate of the vertex was required to be: -50 cm< Z_{vtx} <50 cm. This cut is used to select events which occur close to the nominal interaction point.

7. Track quality cuts, transverse momenta p_t and pseudorapidities η of each track were required to be :

   (a) $p_t > 150$ MeV

   (b) $|\eta| < 1.75$;

   these cuts allow to select only tracks which passed through the high acceptance region of the CTD which is correctly reproduced in the Monte Carlo.

8. Both tracks should correspond to oppositely charged particles.

9. Matching of tracks and CAL energy deposits : The energy deposited in UCAL by a single track was calculated separately in the hadronic and electromagnetic sections, as a sum of all cell energies within a radius of 25 cm (EMC) and of 40 cm (HAC) around the point where the track enters the UCAL. Energy deposited in the most energetic calorimeter cell and not assigned to any of the Φ decay tracks was required

---

[1] The shower width is a measure of the spread in energy depositions around the mean reconstructed position of the positron

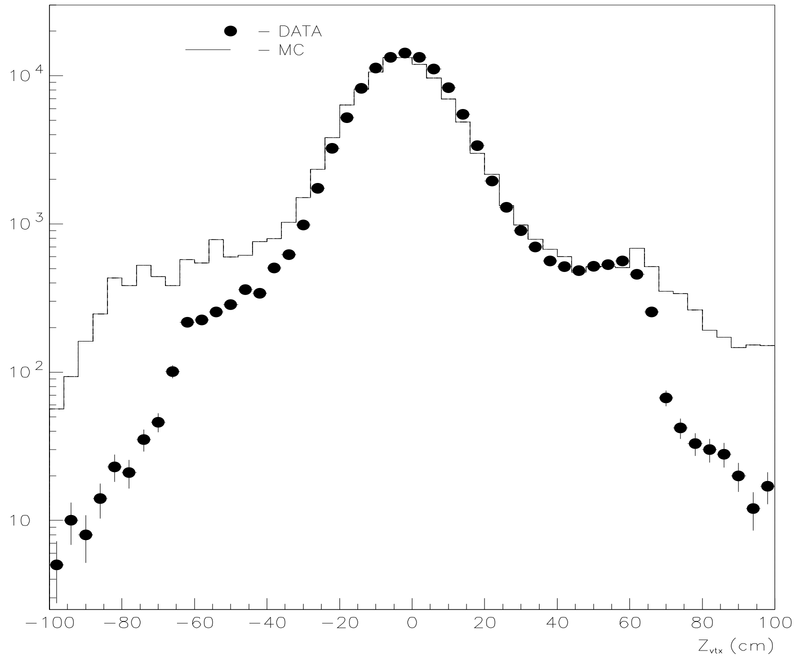

Figure 4.3: *Vertex distribution in data and Monte Carlo. Monte Carlo is normalised to data in range -66 cm < Z_{vtx} < 66 cm.*

to be below a certain value E_{cut}. In this analysis the value of E_{cut} was the same for the HAC and EMC sections of FCAL, BCAL, RCAL and "ring" (10 cm $< |X| <$ 14 cm and 10 cm $< |Y| <$ 14 cm) around the beam-pipe, $E_{cut} =$ 200 MeV, which corresponds to the maximal noise in a single calorimeter cell. The purpose of this cut was to reject events with final state particles in the CAL other then two decay kaons. Such events originate mainly from:

- Proton dissociative events $ep \rightarrow eX\Phi$, where the hadronic state X does not enter the acceptance region of the CTD.
- Decay of neutral particles (mainly vector mesons Φ and ω) in the channel $V^0 \rightarrow X^+X^-X^0$, where neutral particle X^0 does not produce a track in CTD and deposits energy in UCAL.

10. Cuts on kinematical variables. The analysis was restricted to the following ranges of kinematical variables :

    (a) 0.25 GeV^2 $< Q^2 <$ 0.85 GeV^2

    (b) 25.0 GeV $< W <$ 90.0 GeV

    (c) t< 0.6 GeV^2

On Fig. 4.6 the effect of subsequent cuts is shown while Tab. 4.1 gives an overview of performance of the used cuts.

Number of the cut	# events after this cuts	percent of rejected events
4.2.1 AND 4.2.2-1	93000	-
2	66797	28
3	66745	0.07
4	48060	28.0
5	47748	0.6
6	46663	2.3
7a	35898	23.1
7b	21628	39.8
8	19992	7.6
9	5575	72.1
10	4886	12.4
4.2.3	1518	68.9

Table 4.1: *Off-line selection chain.*

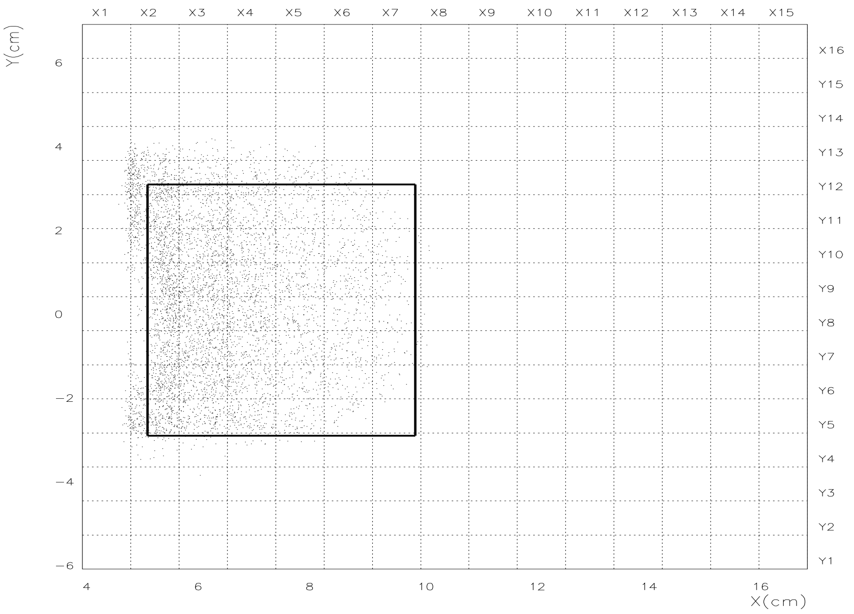

Figure 4.4: *The BPC reconstructed Y position versus reconstructed X position of the positron where all selection cuts except for the fiducial volume cut. The solid line denote fiducial volume area. The dotted horizontal and vertical dotted lines denote the strip boundaries.*

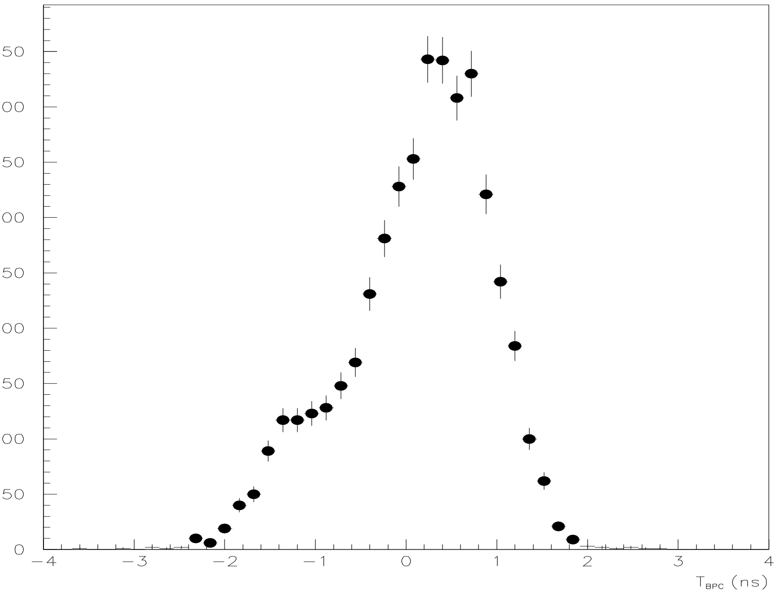

Figure 4.5: *The BPC timing ($T_{BPC} = t_{BPC} - < t_{BPC} >$) distribution in data (for the description of the variables see cut 3).*

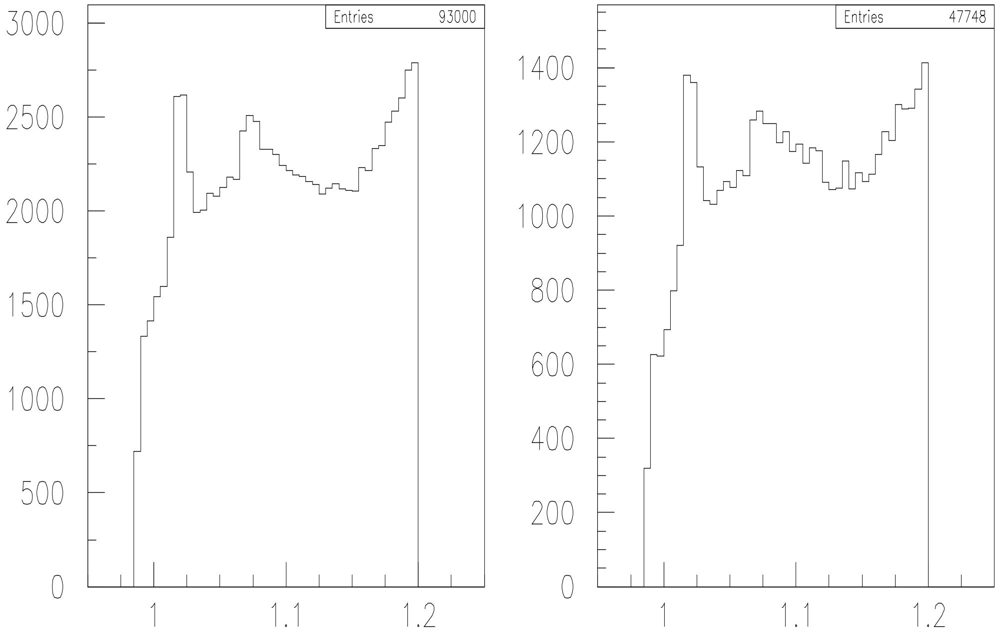

a) M_{K+K-} after online selection (1–3) b) M_{K+K-} after offline selections 1–5

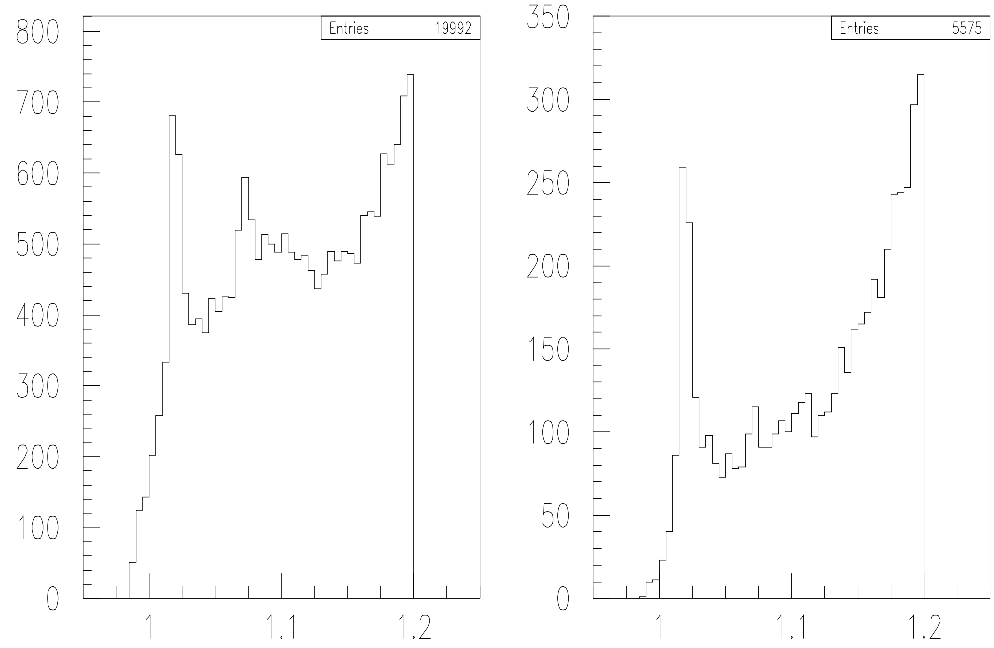

c) M_{K+K-} after offline selections 1–8 d) M_{K+K-} after elasticity cuts 9

Figure 4.6: *Data after subsequent selections described in this section.*

4.2.3 Particle identification (dE/dx)

The energy loss in a given medium depends on the mass of the particle and therefore may be helpful in particle identification. In the low momentum region, p <0.8 GeV, the separation between kaons and pions on the base of dE/dx measurement becomes possible. The dE/dx identification in this analysis was done using the method described below. Fig. 4.7 shows dE/dx as a function of momentum for positive and negative tracks after selections 1-10. Region of large concentration of points, below 1.4 MIP, is mainly due to pions and kaons. Steep vertical correlations of dE/dx and p are due to kaons and protons, as denoted on the figure. On Fig. 4.7a there are only few points due to protons which do not have counterparts on the Fig. 4.7b (antiprotons are not expected to be present in the sample). The theoretical curves show predictions of the Bethe-Bloch formula [45].

Let $\mathcal{L}_i$ denote the absolute probability that the true dE/dx value, $dE/dx_{th}(p)$, of particle of type i (i=e, p, K, p, d) and momentum p was measured as $dE/dx_{data}(p)$:

$$\mathcal{L}_i = exp\left(- \frac{\left(\left(\frac{dE}{dx}\right)^i_{th} - \left(\frac{dE}{dx}\right)_{data} \right)^2}{2\sigma^2} \right) . \tag{4.12}$$

Here σ denotes the resolution of the dE/dx measurement, which was found to be well described by the following formula : $\sigma = a/N_{hits} + b$, where N_{hits} denotes the number of pulses from CTD wires that were used in measurement of the $dE/dx_{data}(p)$ for the given track and a, b are fitted constants [49, 50]. The normalised probability $\mathcal{P}_i$ can be defined as:

$$\mathcal{P}_i = \frac{\mathcal{L}_i}{\sum_{j=e,\pi,K,p,d} \mathcal{L}_j}. \tag{4.13}$$

Both absolute and normalised probabilities can be used to identify particles. The procedure was applied only to those events which occurred during the runs in which the gas pressure in the CTD was monitored [2]. The purpose of the dE/dx identification was to reject a big fraction of background events without loosing $\Phi \to K^+K^-$ events. The event was identified on the basis of the dE/dx information from one of the tracks (tagging track). The identification procedure was applied only to those events in which at least one of the tracks satisfied $N_{hits} \geq 5$. The event was identified as $\Phi \to K^+K^-$ and accepted if it satisfied the following requirement :

$$\mathcal{L}_{tagger} > \mathcal{L}_{cut} \qquad OR \qquad \mathcal{P}_{tagger} > \mathcal{P}_{cut} \tag{4.14}$$

where the tagging track was chosen as follows :

---

[2] This is due to pressure corrections which require gas pressure information

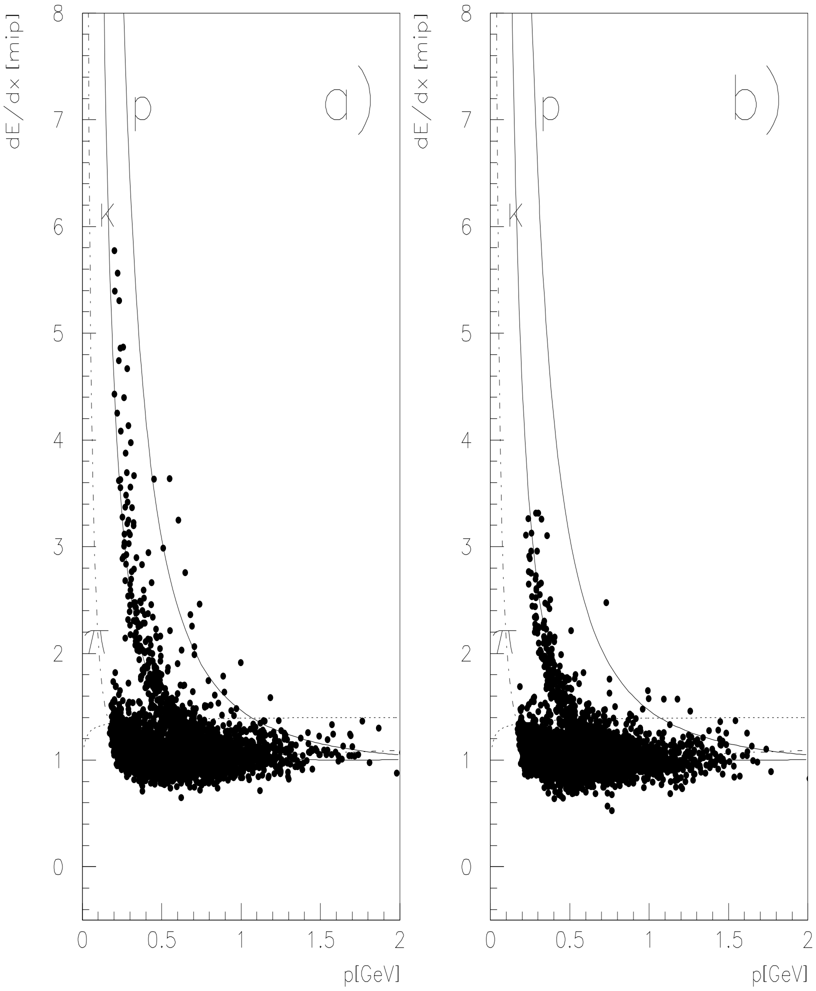

Figure 4.7: *Scatter plot of dE/dx vs. p with superimposed theoretical curves based on the Bethe-Bloch formula for different species of particles, (a) tracks corresponding to positive particles ; (b) tracks corresponding to negative particles.*

1. If each track fulfilled $N_{hits} \geq 5$, the lower momentum track was chosen as a tagging track.
2. In the case of only one track satisfying $N_{hits} \geq 5$, this particular track was chosen as a tagging track.

In the present analysis the following values were adopted : $\mathcal{L}_{cut} = 0.01$ and $\mathcal{P}_{cut} = 0.2$, which allow to retain all $\Phi \to K^+K^-$ events. Fig. 4.8a shows dE/dx versus momentum of the tagging track if accepted by the above criteria. On Fig. 4.8b the dE/dx as a function of momentum of the other track (not tagging track) which were rejected is shown. Since no remnant of the kaon band is present in Fig. 4.8b one may conclude that the procedure

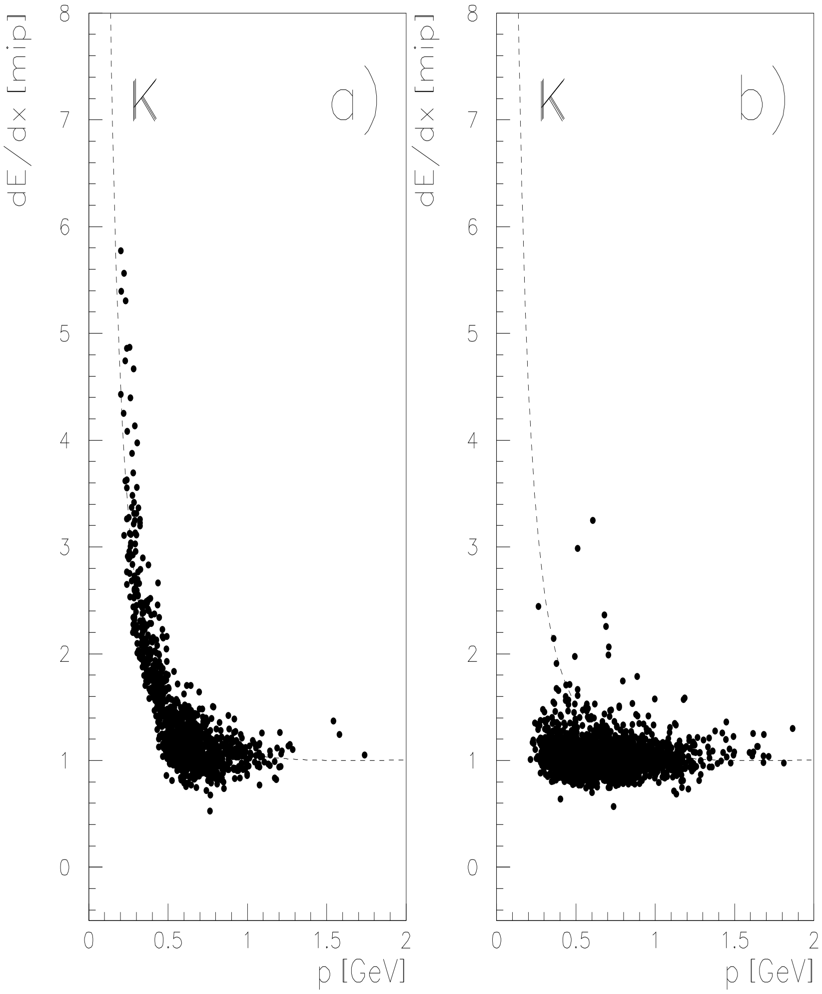

Figure 4.8: *dE/dx as a function of p of (a) accepted tagging tracks ; (b) rejected not tagging track.*

of identification do not affect the $\Phi \to K^+K^-$ signal.

The background rejection with the dE/dx identification method is not 100% efficient. The efficiency of the background rejection was determined as follows. Because Φ is a very narrow resonance ($\Gamma = 4.43$ MeV), events in which $M_{KK} > 1.075$ GeV are background events (Fig. 4.10a). These events can be used to determine the efficiency of background rejection which is defined as follows:

$$\varepsilon = \frac{N_{rejected}^{1.075<Mkk<1.2}}{N_{total}^{1.075<Mkk<1.2}} = 0.77 \pm 0.01. \tag{4.15}$$

where $N_{total}^{1.075<Mkk<1.2}$ denotes the total number events in the range 1.075 GeV $< M_{KK} <$ 1.2 GeV and $N_{rejected}^{1.075<Mkk<1.2}$ denotes the number of events identified as background events and rejected. Fig. 4.9 shows the efficiency of rejecting background events as a function of invariant mass M_{KK} of two tracks. It follows from this figure that the efficiency does not depend on M_{KK}. Thus assuming it is also constant in the M_{KK} region under the Φ peak, number of Φ events, N_Φ, in the certain M_{KK} interval can be determined from the following formula :

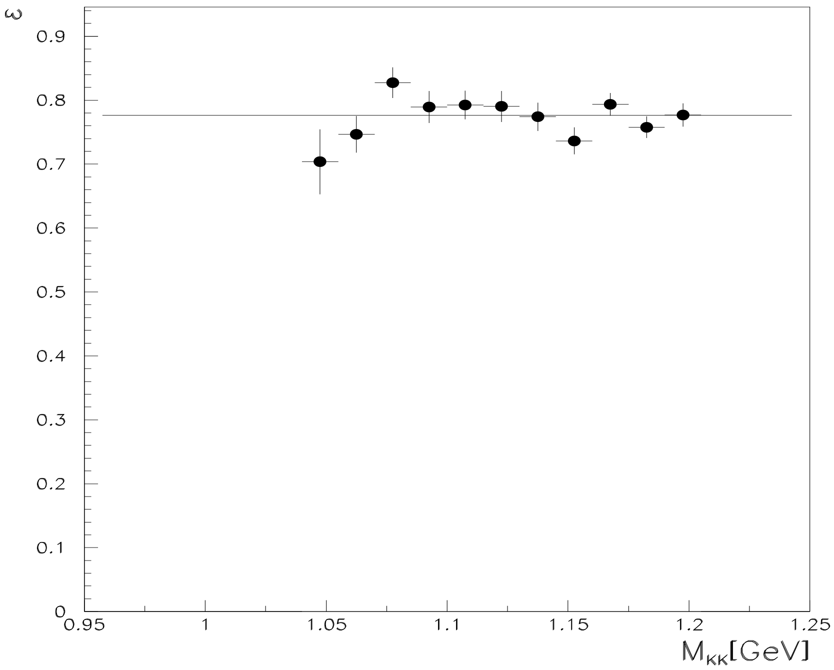

Figure 4.9: *Efficiency of rejecting background in function of* M_{KK}.

$$N_\Phi = N_{total} - \frac{N_{rejected}}{\varepsilon} \tag{4.16}$$

Because the efficiency of background rejection, ε, depends strongly on the momentum of the tagging track, it also depends on W. Thus the numbers of Φ events in three W bins (25< W <40, 40< W <60, 60< W <90) were determined using three different values of ε. They were calculated according to Eq. 4.15 with an additional cut on W and are presented in table below.

W range	ε
20 - 40	0.74±0.01
40 - 60	0.91±0.01
60 - 90	0.52±0.02

4.2.4 Final data sample

In the later analysis the two alternative data samples were considered. The cross section has been determined using the following data samples:

- after selections (1-10) with no dE/dx particle identification, Fig. 4.10.
- after selections (1-10) and dE/dx particle identification, Fig. 4.11

In order to get rid of large amount of background events (Fig. 4.11) and restrict the analysis to the region where background contribution was relatively small ($\approx 15\%$, see Sec. 6) an additional cut on invariant mass, 1.00 GeV $< M_{KK} <$ 1.04 GeV, was imposed.

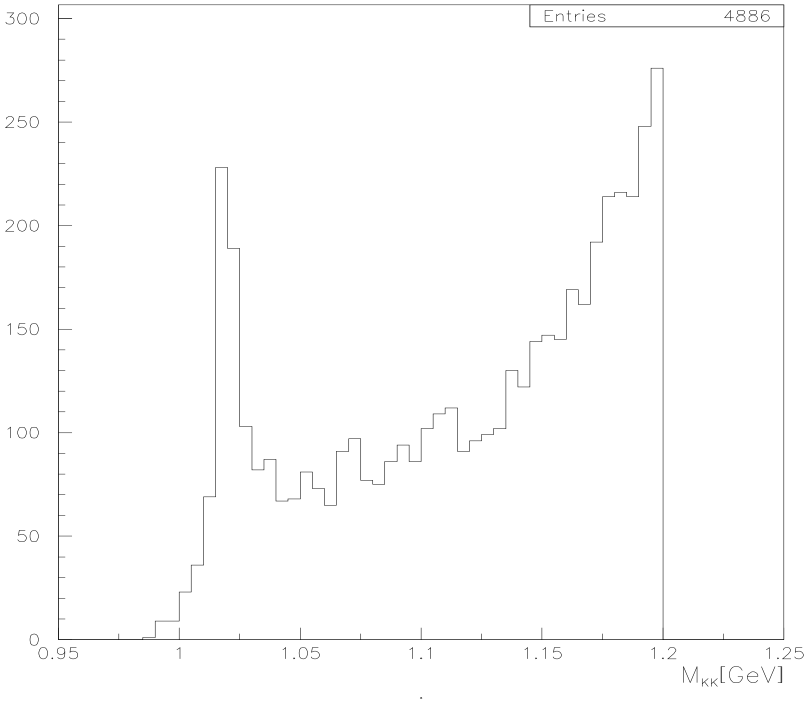

Figure 4.10: *Data sample after selections 1-10.*

4.3 Dominant background sources

4.3.1 Production of other particles

All the background processes described below are present in the both final data samples (Fig. 4.10, Fig. 4.11) but their contribution to the data sample after dE/dx identification is significantly smaller.

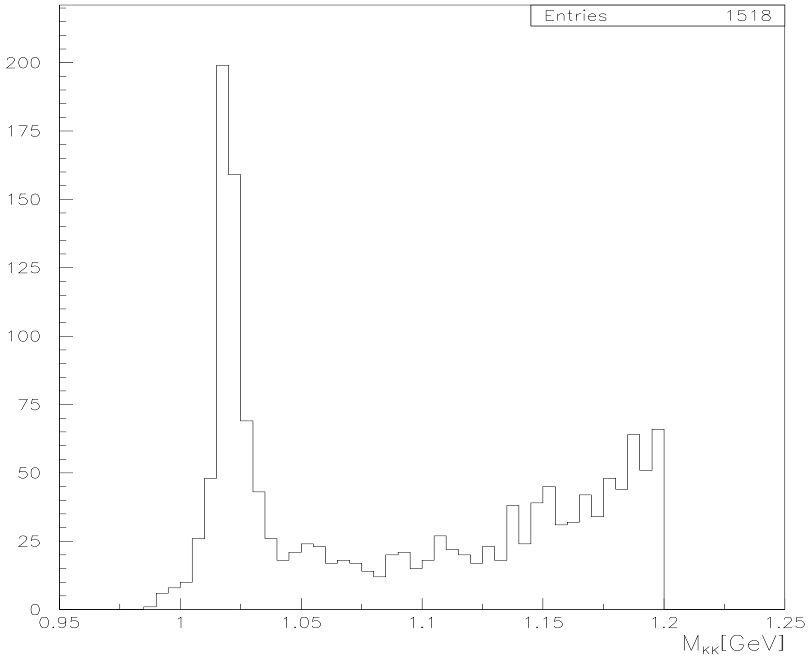

Figure 4.11: *Data sample after selection 1-10 and dE/dx particle identification.*

- $\rho \to \pi^+\pi^-$
  This is the dominant source of background, two pion tracks are misidentified as kaon tracks.

- $\omega \to \pi^+\pi^-\pi^0$,$\Phi \to \pi^+\pi^-\pi^0$
  This backgrounds are strongly suppressed by cuts 4.2-8, because of π^0 which deposits energy in UCAL which is not matched to any track.

- $\bar{K^0}(K^0) \to \pi^+\pi^-$
  Signal from $\bar{K^0}, K^0$ is clearly visible at the $M_{KK}\simeq$ 1.075 (Fig. 4.10).

- Nonresonant K^+K^- pair production

Fig. 4.13 shows the final data sample before applying the dE/dx identification procedure with the Monte Carlo simulated for several background processes described above after applying similar selection criterias. The Monte Carlo have been normalised to the data as follows :

1. $\rho \to \pi^+\pi^-$ in the invariant mass region 1.19 GeV $< M_{KK} <$ 1.2 GeV.

2. $\omega \rightarrow \pi^+\pi^-\pi^0$ according to the prediction : $\sigma_{\rho^0} : \sigma_\omega$=9:1, which is in good agreement with the ZEUS 94 measurement [23] $\sigma_{\rho^0} : \sigma_\omega = 14.5 \pm 5.0$. Number of ρ^0 events found in 1° has been used.

3. $\Phi \rightarrow \pi^+\pi^-\pi^0$ using the acceptance corrected number of $\Phi \rightarrow K^+K^-$ events (see Sec. 6) and branching ratio for the $\Phi \rightarrow \pi^+\pi^-\pi^0$ decay, $B' \simeq 15.6\%$.

4. $\bar{K^0}(K^0) \rightarrow \pi^+\pi^-$ to the $\bar{K^0}(K^0)$ peak region 1.065 GeV $< M_{KK} <$ 1.075 GeV

The sum of contributions to the final sample coming from the above processes is shown on Fig. 4.14.

4.3.2 Proton dissociative background

The dominant source of the background in the final sample are the proton dissociative events. These are the events where the incoming proton does not keep its identity as in the elastic case and dissociates into the hadronic state X (Fig. 4.12). A typical signature of such event is shown on Fig. 4.15. Significant part of these events is rejected by elasticity cuts (4.2.2-9), but a fraction escapes detection. The contribution from proton dissociative events to the final sample depends mainly on the matching procedure and elasticity selection criterias that were used in the analysis. The amount of this background has been adopted from earlier exclusive ρ^0 analysis [5, 16] in which similar matching procedure and elasticity cuts has been used. According to these analysis the fraction of the proton dissociative events in the final sample amounts to $C_{diss} = 24.0 \pm 7.5\%$.

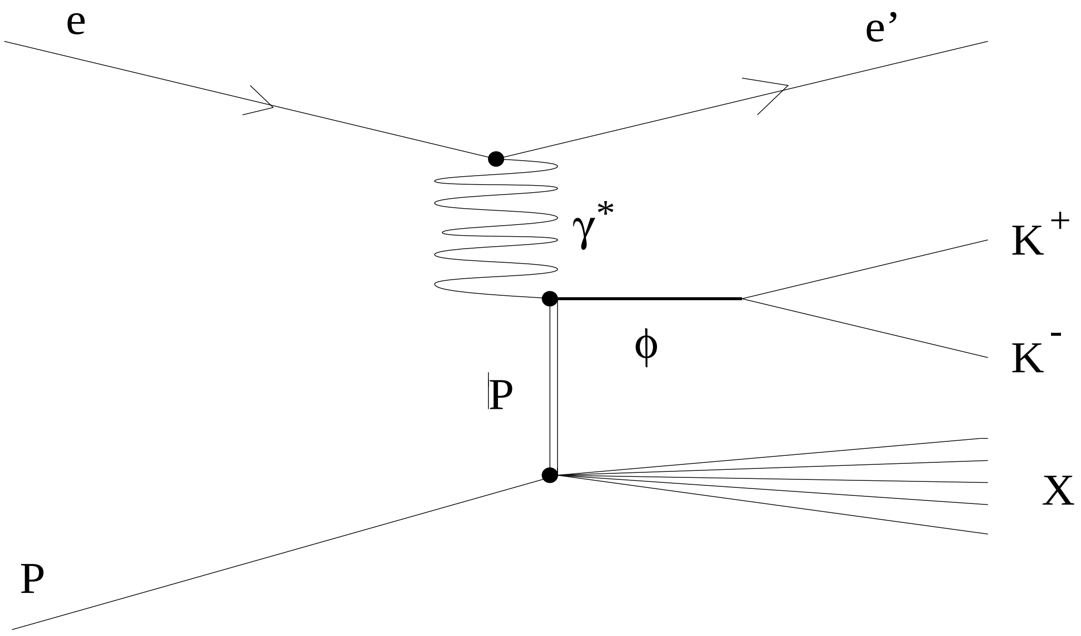

Figure 4.12: *Diagram of Φ meson electroproduction with proton dissociation.*

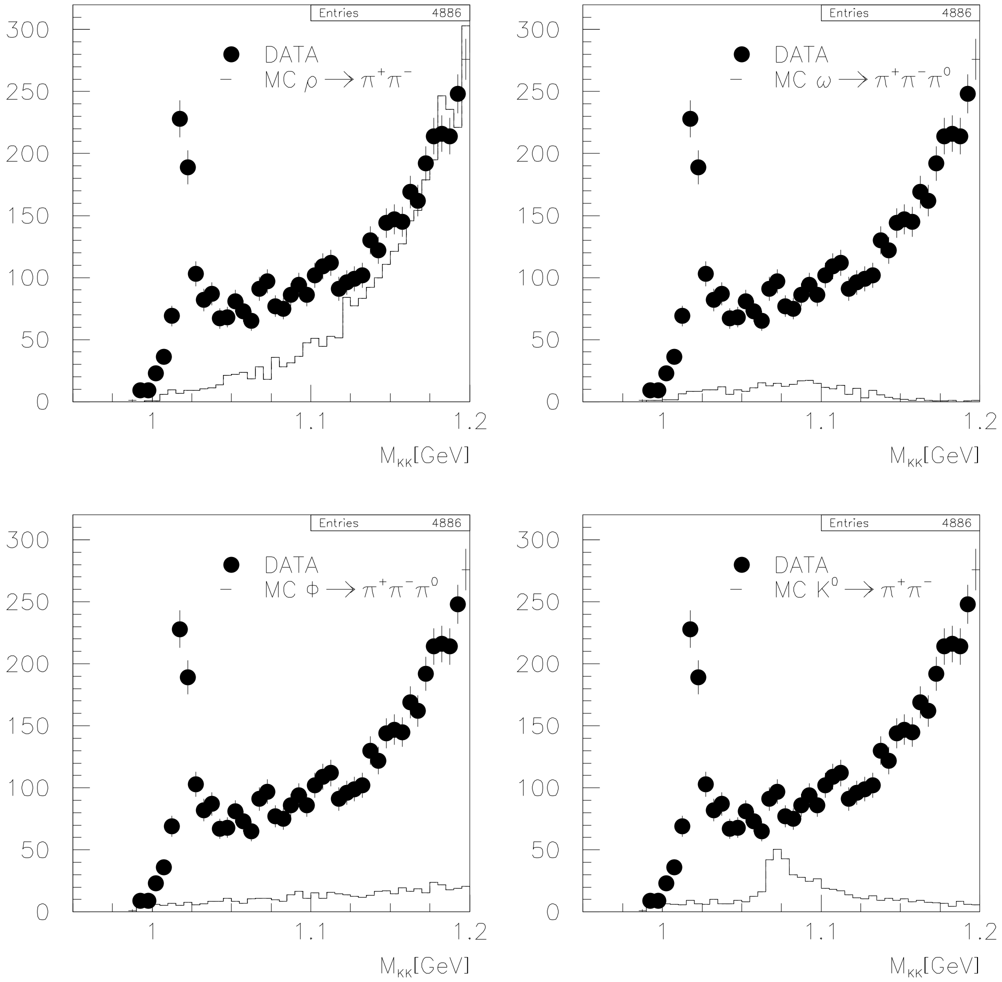

Figure 4.13: *Contribution from different background processes.*

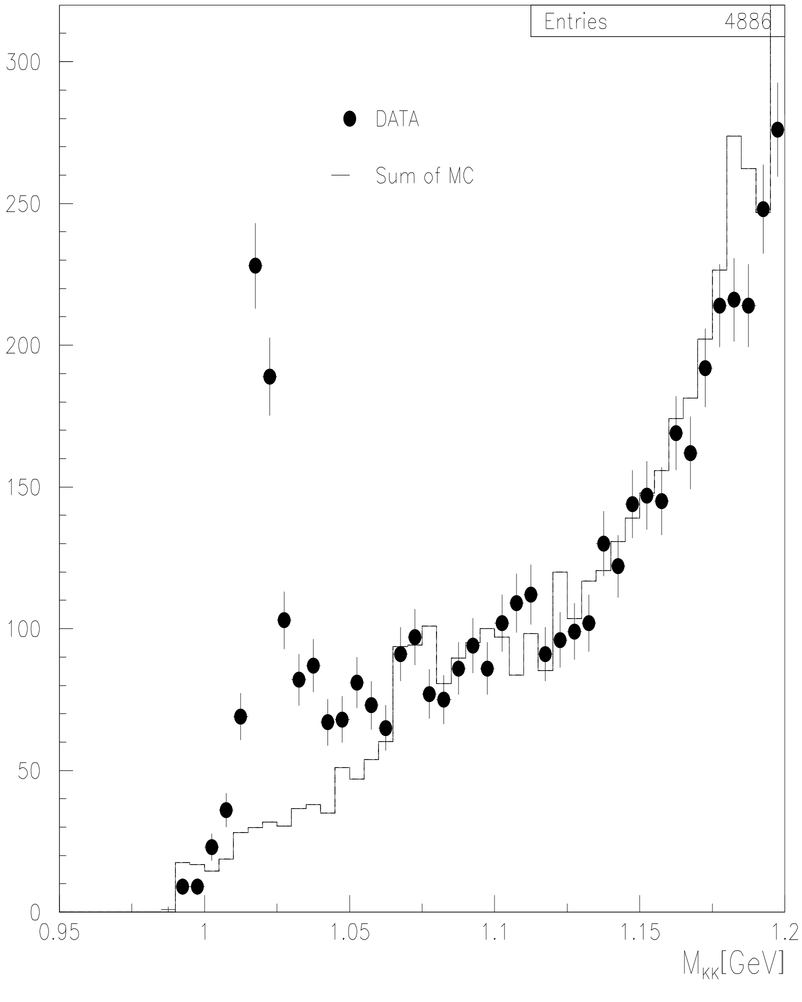

Figure 4.14: *The sum of four background contributions ($\rho \to \pi^+\pi^-$, $\omega \to \pi^+\pi^-\pi^0$, $\Phi \to \pi^+\pi^-\pi^0$, $\bar{K^0}(K^0) \to \pi^+\pi^-$).*

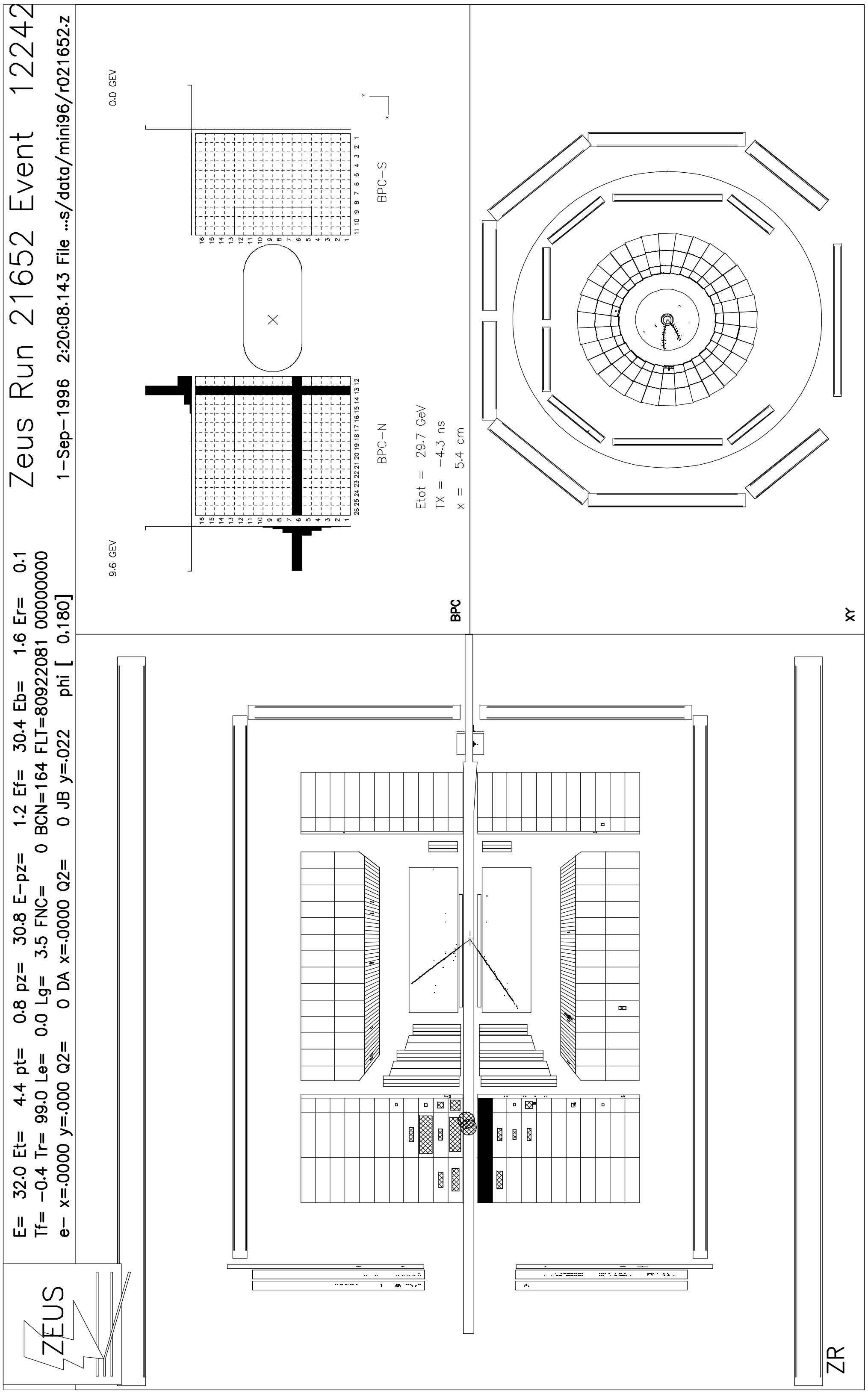

Figure 4.15: *Proton dissociative Φ electroproduction event with displayed using program LAZE. The hadronic state X deposits energy in FCAL, around the beampipe.*

Chapter 5

Data analysis

5.1 Monte Carlo simulation

Monte Carlo (MC) simulation of the physical process and the ZEUS detector is necessary to correct for acceptance and efficiencies of the detector and software reconstruction. The simulation of the studied process can be divided in to three steps :

- Events are generated according to our actual knowledge of the underlying physics (cross sections, angular distributions etc.).
- Each particle is tracked through the detector and the response of the various components is simulated.
- The trigger is simulated. The generated events are reconstructed using the same software as for the data events.

In the present analysis, a dedicated Monte Carlo generator was used [60, 58]. The main physical assumptions are listed below :

1. Cross sections for the process $\gamma^* p \to \Phi p$ were parametrised according to the VMD model and Regge phenomenology (Sec. 2.3.1 and 2.3.2). Thus the double differential cross section, $d\sigma/dQ^2dy$, for the $ep \to e\Phi p$ had the following form :

$$\frac{d^2\sigma}{dQ^2dy}(Q^2, y) \propto \frac{W^{0.2}}{yQ^2 \cdot (1 + M_\Phi^2/Q^2)^2} \tag{5.1}$$

2. t dependence of the differential cross section according to ZEUS 94 Φ photoproduction measurement [6]: $d\sigma/dt \propto e^{-bt}$, where $b = 7$ GeV^{-2}.
3. shape of the Φ resonance was parametrised by a relativistic p-wave Breit-Wigner function (see Eq. 5.11)
4. angular distributions - according to SCHC hypothesis (Eq. 2.36).

The experimental resolution of kinematical variables in the final sample has been determined from distribution (Fig. 5.1) of the variable :

$$\Delta V = V_{generated} - V_{reconstructed} \ ,$$

where V denotes M_{KK}, Q^2, W, t, $cos\theta_h$ or ϕ_h. The study of the experimental resolution is necessary to choose correct bin widths in distributions of the kinematical variables. On the Fig. 5.1 results of fitting the following parameterisation of the resolution are also shown :

$$\sigma_V = N_1 \cdot exp\left(-\frac{(\Delta V - m_1)^2}{2\sigma_1}\right) + N_2 \cdot exp\left(-\frac{(\Delta V - m_2)^2}{2\sigma_2}\right) \ . \tag{5.2}$$

Variable	N_1	m_1 (MeV)	σ_1 (MeV)	N_2	m_2 (MeV)	σ_2 (MeV)
M_{KK}	211.4±9.49	-0.34 ± 0.06	1.64 ± 0.08	24.44 ± 5.26	-0.9 ± 0.31	4.84 ± 0.34
Q^2	107.19±31.7	-0.63 ± 2.37	9.01 ± 0.54	36.67 ± 35.27	-10.67 ± 3.81	6.96 ± 1.49
W	35.18±4.92	204.95 ± 31.17	585.88 ± 36.12	306.65 ± 13.91	27.63 ± 6.55	158.9 ± 7.13
t	126.56±7.6	1.04 ± 0.26	5.16 ± 0.36	35.32 ± 5.48	2.94 ± 0.63	14.24 ± 0.72
$\cos\theta_h$	16.59±3.84	-0.0007 ± 0.004	0.070 ± 0.008	186.86 ± 8.1	-0.0003 ± 0.0007	0.018 ± 0.001
ϕ_h	23.91±5.19	0.006 ± 0.007	0.140 ± 0.013	209.66 ± 9.68	-0.001 ± 0.001	0.040 ± 0.002

Table 5.1: *Results of fitting the resolution function given by Eq. 5.2 to the distribution of ΔV (defined above) in the Monte Carlo.*

According to the obtained results the following bin widths has been chosen : ΔM_{KK}=5 MeV, ΔQ^2=0.06 GeV^2, ΔW = 0.5 GeV, Δt = 0.1 GeV^2, $\cos\theta_h$ = 0.1. The chosen bin width of M_{KK} is comparable to the obtained resolution in M_{KK}, but this will be taken into account in the fitting procedure (see Sec. 5.4).

Fig. 5.2 shows distributions of kinematical variables in data and MC. The MC simulation gives a good description of data. The disagreement which can be seen in the t distribution at $t > 0.5$ GeV^2 is due to the presence of the proton dissociative background in the data, which is not accounted for in the MC. The analysis was restricted to $|t| < 0.6$ GeV^2 and the global correction for the proton dissociative background was made (Sec. 4.3.2).

5.2 Acceptance determination

The acceptance coefficient of a variable V in a certain range of values, $[V_{min}, V_{max}]$, can be defined as follows :

$$A^{[V_{min},V_{max}]} = \left\{\frac{\#Events\ passing\ selections\ [V_{min}, V_{max}]}{\#Events\ generated\ [V_{min}, V_{max}]}\right\}_{MC}$$

Fig. 5.3 shows acceptance functions of different kinematical variables. The overall acceptance for the elastic Φ events in the selected range of kinematical variables , 0.25 GeV$<^2$ $Q^2 < 0.85$ GeV^2, 25 GeV $< W <$ 90 GeV, $|t| < 0.6$ GeV^2, was determined to be :

$$A_{tot} = 0.0312 \pm 0.0008\ .$$

Small value of this acceptance is mainly due to the fact that the BPC fiducial area covers only a small part ($\simeq 13\%$) of the solid angle corresponding to the above kinematical range (Sec. 3.2.3).

5.3 Method of evaluation of the cross sections

The $\gamma^* p \to \Phi p$ cross section has been evaluated using Eq. 2.16 :

$$\sigma_{\gamma^* p \to \Phi p}(Q_0^2, y_0) = \frac{1}{\Gamma} \frac{d^2\sigma_{\gamma p \to \phi p}}{dQ^2 dy}(Q_0^2, y_0)\ . \tag{5.3}$$

Finite binning in the data allows to determine :

$$\left(\frac{\Delta\sigma_{ep \to \phi ep}}{\Delta Q^2 \Delta y}\right)_{DATA} = \frac{N^{bin}}{A \cdot L_{int} \cdot \Delta Q^2 \Delta y}\ , \tag{5.4}$$

where N^{bin} denotes number of events in a given (Q^2, y) interval, L_{int} integrated luminosity and A acceptance.

In order to determine double differential cross section, $(d^2\sigma_{\gamma p \to \phi p}/dQ^2 dy)_{DATA}(Q_0^2, y_0)$, from the measured $(\Delta\sigma_{ep \to \phi ep}/\Delta Q^2 \Delta y)_{DATA}$ the following relation may be used:

$$\left(\frac{d^2\sigma_{\gamma p \to \phi p}}{dQ^2 dy}\right)_{DATA}(Q_0^2, y_0) = \left(\frac{\Delta\sigma_{ep \to \phi ep}}{\Delta Q^2 \Delta y}\right)_{DATA} \cdot \frac{\left(\frac{d^2\sigma_{\gamma p \to \phi p}}{dQ^2 dy}\right)_{MC}(Q_0^2, y_0)}{\left(\frac{\Delta\sigma_{ep \to \phi ep}}{\Delta Q^2 \Delta y}\right)_{MC}}\ , \tag{5.5}$$

where $(d^2\sigma_{\gamma p \to \phi p}/dQ^2 dy)_{MC}(Q_0^2, y_0)$ is the parametrisation of the cross section used in the Monte Carlo (Eq. 5.1) and $(\Delta\sigma_{ep \to \phi ep}/\Delta Q^2 \Delta y)_{MC}$ can be calculated as follows :

$$\left(\frac{\Delta\sigma_{ep \to \phi ep}}{\Delta Q^2 \Delta y}\right)_{MC} = \frac{1}{\Delta Q^2 \Delta y} \int_{\Delta Q^2, \Delta y} \left(\frac{d^2\sigma_{\gamma p \to \phi p}}{dQ^2 dy}\right)_{MC}(Q^2, y) dQ^2 dy\ , \tag{5.6}$$

where integration is performed over the $(\Delta Q^2, \Delta y)$ bin. Thus the double differential cross section in certain point (Q_0^2, y_0), belonging to the $(\Delta Q^2, \Delta y)$ bin, can be determined from the following formula :

$$\left(\frac{d^2\sigma_{\gamma p \to \phi p}}{dQ^2 dy}\right)_{DATA}(Q_0^2, y_0) = \frac{N^{bin}}{A \cdot L_{int}} \bar{f}(Q_0^2, y_0)\ , \tag{5.7}$$

where $\bar{f}(Q_0^2, y_0)$ is defined as follows :

$$\bar{f}(Q_0^2, y_0) = \frac{\left(\frac{d^2\sigma_{\gamma p \to \phi p}}{dQ^2 dy}\right)_{MC}(Q_0^2, y_0)}{\int_{\Delta Q^2, \Delta y} \left(\frac{d^2\sigma_{\gamma p \to \phi p}}{dQ^2 dy}\right)_{MC}(Q^2, y) dQ^2 dy}\ . \tag{5.8}$$

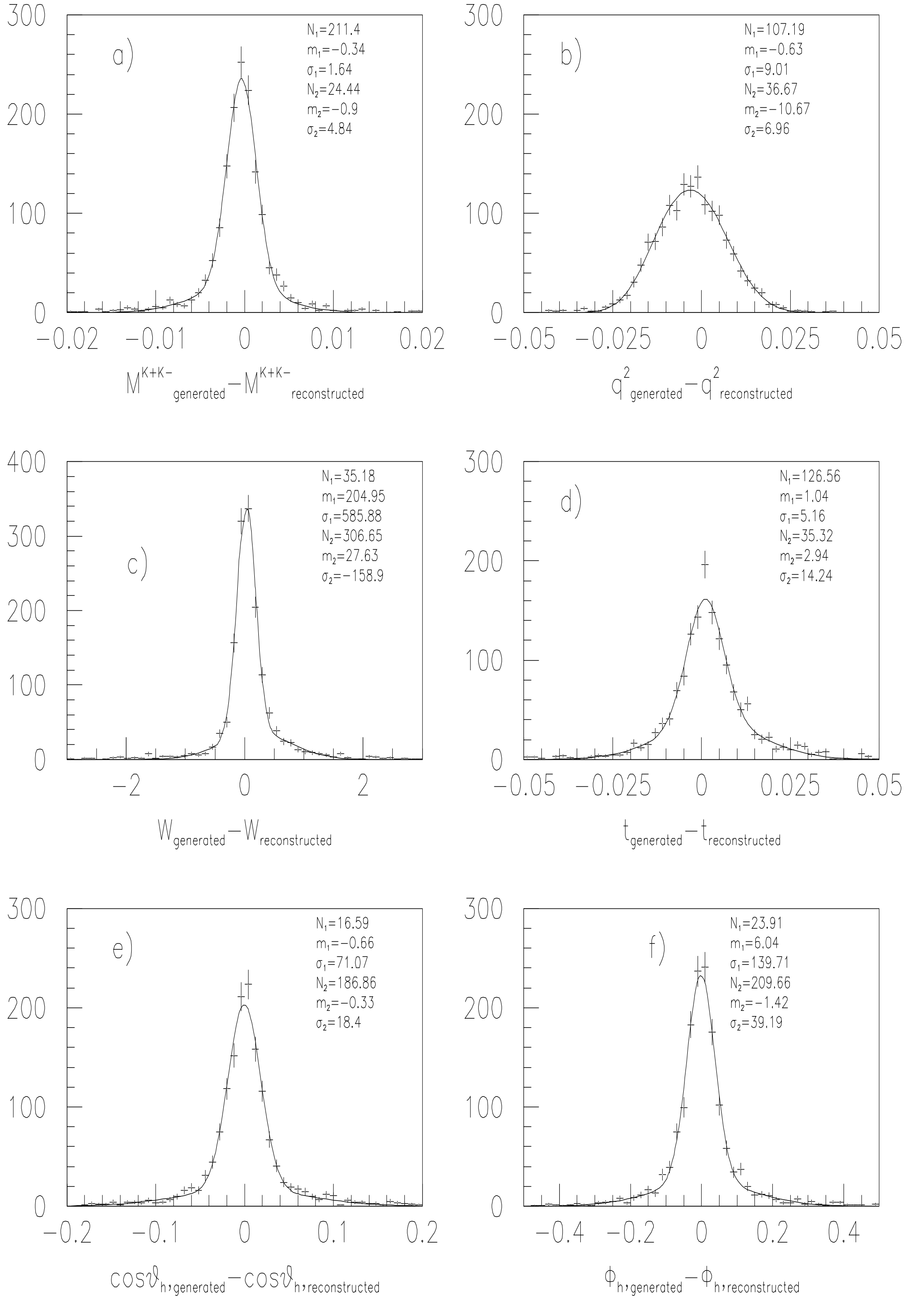

Figure 5.1: *Experimental resolution of different variables (a) M_{KK} ; (b) Q^2 ; (c) W ; (d) t ; (e) $\cos\theta_h$; (f) ϕ_h. Figure shows Monte Carlo after applying selections 1-10 (Sec. 4.2).*

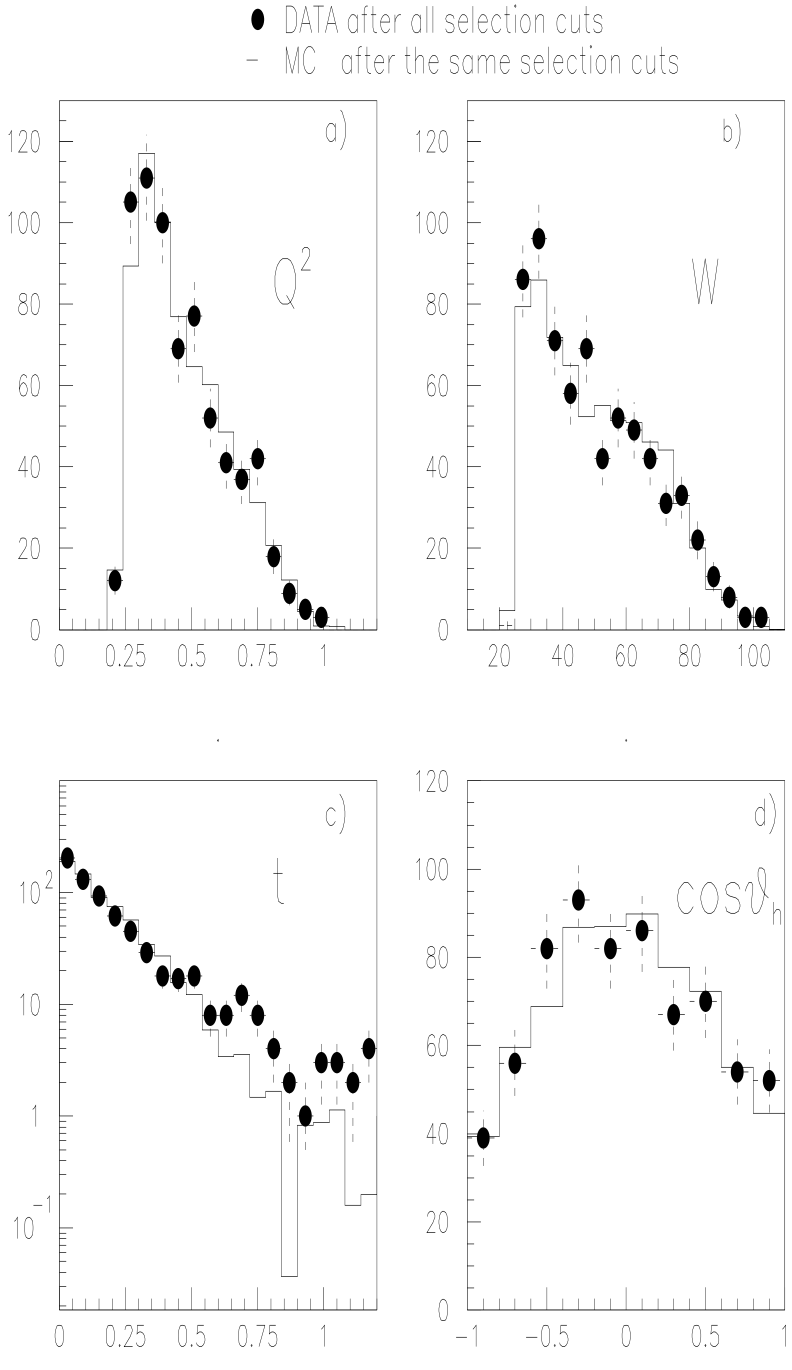

Figure 5.2: *Comparison of reconstructed kinematical variables in data and Monte Carlo : (a)*Q^2 *; (b)*W*; (c)*t *; (d)* $\cos\theta_h$.

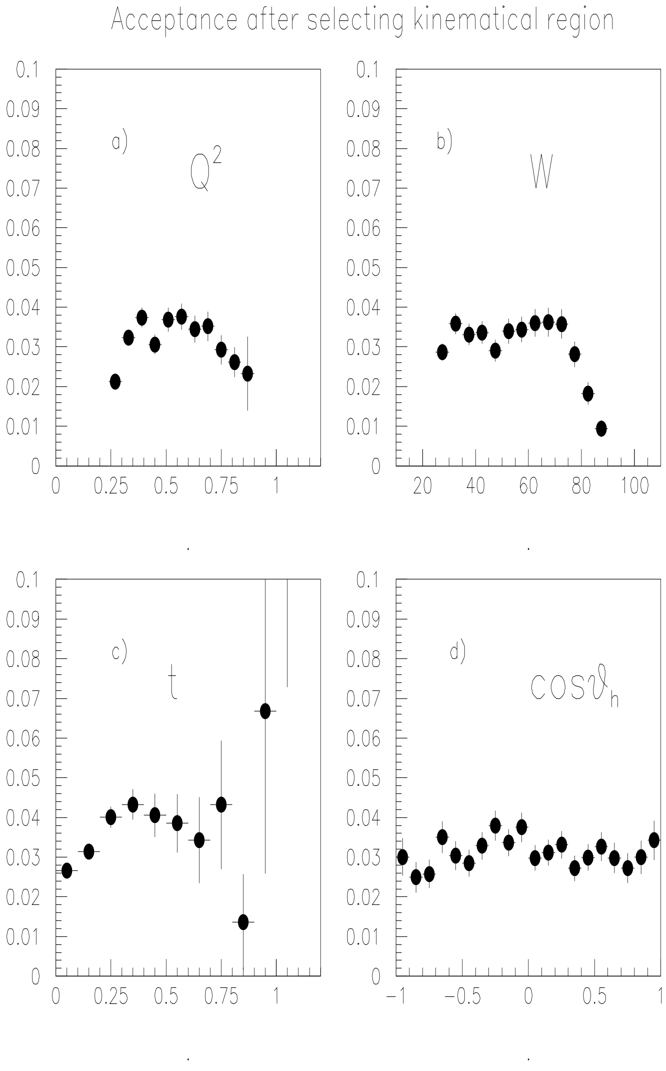

Figure 5.3: *Acceptance functions of following kinematical variables : (a)* Q^2 *; (b)* W *; (c)* t *; (d)* $cos\theta_h$.

In the present analysis the double differential cross section was determined in the centre of a given $(\Delta Q^2, \Delta y)$ bin. In the case of the exclusive Φ analysis in the K^+K^- decay channel, N^{bin} from the Eq. 5.7 can be expressed as :

$$N^{bin} = \frac{N_\Phi \cdot (1 - C_{diss})}{B} , \tag{5.9}$$

where C_{diss} denotes the fraction of the proton dissociation background, B is a branching ratio for the $\Phi \to K^+K^-$ channel and N_Φ is a number of observed Φ events in a certain $(\Delta Q^2, \Delta y)$ bin. After substituting the above formula to Eq. 5.7 the following final formula is obtained :

$$\left(\frac{d^2\sigma_{\gamma p\to\phi p}}{dQ^2 dy}\right)_{DATA} (Q_0^2, y_0) = \frac{N_\Phi \cdot (1 - C_{diss})}{L_{int} \cdot A \cdot B} \cdot \bar{f}(Q_0^2, y_0). \tag{5.10}$$

Number of observed Φ events, N_Φ, was calculated in the invariant mass interval 1.00 GeV $< M_{KK} <$ 1.04 GeV, using two alternative methods :

1. dE/dx identification with the efficiency correction (Sec. 4.2.3), the results for the N_Φ and N_B (number of background events in the invariant mass interval 1.00 GeV $< M_{KK} <$ 1.04 GeV) are as follows : $N_\Phi = 512.0 \pm 35.0$, $N_B = 308.0 \pm 20.0$
2. from fitting Breit-Wigner (BW) function, this method will be described in the next section.

5.4 Determination of the total number of Φ events.

All the mass fits presented in this section were performed in the invariant mass range 0.99 GeV $< M_{KK} <$ 1.09 GeV. The Φ resonance in the K^+K^- spectrum was parametrised by the relativistic p-wave Breit-Wigner function [40]:

$$BW(M_{KK}) = F \frac{M_{KK} M_\Phi \Gamma_\Phi}{(M_{KK}^2 - M_\Phi^2)^2 + M_\Phi^2 \Gamma_\Phi^2} , \tag{5.11}$$

where M_Φ is the nominal Φ mass, F is the normalisation factor and Γ_Φ is the momentum dependent width :

$$\Gamma_\Phi = \Gamma_0 \left(\frac{p^*}{p_0^*}\right)^3 \frac{M_\Phi}{M_{KK}} , \tag{5.12}$$

where Γ_0 is the nominal width of Φ meson , q^* is the momentum of the decay kaon in the K^+K^- rest frame and q^0 is the value of the kaon momentum at the nominal M_Φ mass :

$$q^* = \sqrt{\left(\frac{M_{KK}}{2}\right)^2 - m_K^2} \qquad q^0 = \sqrt{\left(\frac{M_\Phi}{2}\right)^2 - m_K^2}. \tag{5.13}$$

Because the width of Φ meson (Γ_0 = 4.43 MeV) is comparable with the invariant mass resolution, estimated with the MC (Sec. 5.1) to be $\sigma_m \approx$ 5.0 MeV, the Breit-Wigner function that describes shape of Φ resonance must be convoluted with a resolution function in order to describe the experimental shape :

$$BWR(m) = \int_{m-6\sigma_m}^{m+6\sigma_m} BW(m')R(m-m')dm' \ . \tag{5.14}$$

The resolution in the Monte Carlo was well described by the sum of the two Gaussians (Sec. 5.1). Thus a following form of the resolution function has been assumed :

$$R(m-m') = \frac{r}{1+r} \cdot exp\left(-\frac{(m-m')^2}{2\sigma_1}\right) + \frac{1}{1+r} \cdot exp\left(-\frac{(m-m')^2}{2\sigma_2}\right) \ , \tag{5.15}$$

where r is the ratio between the two Gaussians and has been either fixed to the value obtained from the Monte Carlo $r = N_1/N_2$=8.65 (method IIa, IIc) or treated a free parameter of the fit (method IIb, IId). Number of the Φ events in the entire kinematical range was determined from the final sample before (method IIa, IIb) or after (method IIc, IId) dE/dx identification. However number of the Φ events in the Q^2 and W intervals has been determined by fitting to the invariant mass distribution, M_{KK}, of the final sample after dE/dx identification (method IIc). In the all cases background was parametrised as follows :

$$BG(M_{KK}) = \alpha(M_{KK} - 2m_K)^\beta \ . \tag{5.16}$$

Thus the shape of the fitted function was the following :

$$N(M_{KK}) = \int_{M_{KK}-0.5\Delta m}^{M_{KK}+0.5\Delta m} \left(BWR(m') + BG(m')\right) dm' \ , \tag{5.17}$$

where Δm denotes the width of the M_{KK} bin. The number of Φ events was calculated in the mass range 1.0 GeV < M_{KK}< 1.04 GeV. Fig. 5.4a,b shows the final data samples with the fitted function (method IIa, IIc). The results of the fits are summarised in the Tab. 5.4, where N_Φ and N_B denote, respectively, number of Φ and background events in the invariant mass range 1.0 GeV < M_{KK}< 1.04 GeV. Fig. 5.5 shows final data sample before applying dE/dx identification with fitted background function and efficiency corrected M_{KK} distribution of events rejected by dE/dx identification.

Method	N_Φ	N_B	M_Φ(GeV)	σ_1(MeV)	σ_2(MeV)	β	r	χ^2
IIa	504.0± 31.0	283.0±18.0	1.0196 ±0.0003	2.3 ± 0.3	8.1 ± 3.0	0.081 ± 0.06	8.65	28.6/17
IIb	516.0± 27.0	276.0± 11.0	1.0196 ±0.0003	1.1 ± 1.5	7.1 ± 1.3	0.84 ±0.04	2.0 ± 13.0	27.6/16
IIc	497.0± 27.0	75.0 ± 13.0	1.0196 ± 0.000 2	2.3 ± 0.2	11.6 ± 7.0	0.40 ± 0.14	8.65	13.89/17
IId	504.0± 27.0	73.0±11.0	1.0196±0.0002	1.1 ± 12.0	8.0± 2.0	0.42 ± 0.13	2.2 ± 1.0	12.03/16

Table 5.2: *Results of the four different methods of determining N_Φ in the entire kinematical range : (IIa) fit before dE/dx and $r = const$; (IIb) fit before dE/dx and $r \neq const$; (IIc) fit after dE/dx and $r = const$; (IId) fit after dE/dx and $r \neq const$.*

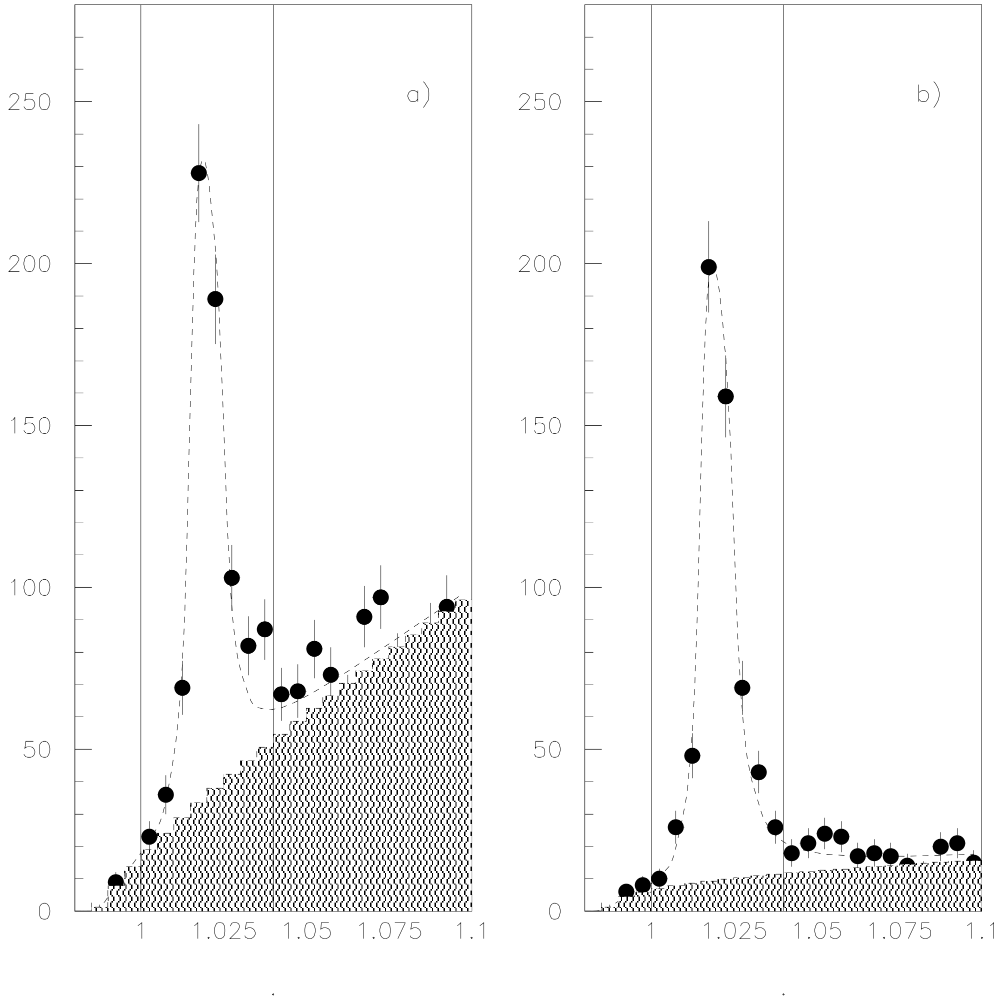

Figure 5.4: *Invariant mass distribution in the final sample : (a) before dE/dx ; (b) after dE/dx with the fitted function.*

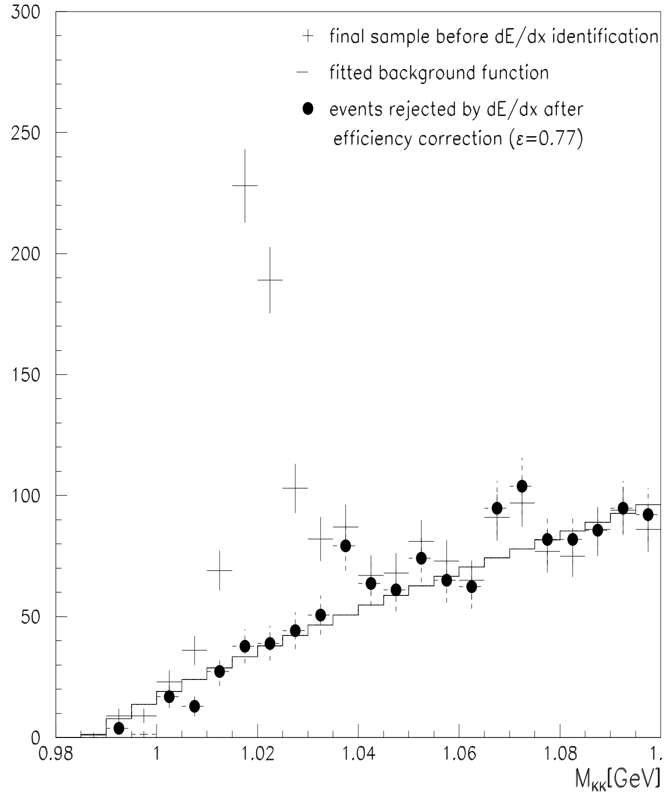

Figure 5.5: *Comparison between the M_{KK} efficiency corrected distribution of events rejected by the dE/dx cut and fitted background function*

Chapter 6

Results

6.1 Systematic Errors

The following systematic checks have been performed :

1. The method of reconstruction of kinematic variables has been changed. Instead of the constrained method (Sec. 4.1) the electron method was used for calculating Q^2, W and t.
2. The cut on the transverse momentum of the kaon tracks was moved from the nominal value of 150 MeV to 100 MeV and 200 MeV.
3. The cut on pseudorapidity η of the reconstructed tracks was moved from 1.75 to 1.5 and 2.0.
4. The cut on the Z position of the reconstructed vertex was moved from 50 cm to 40 cm and 60 cm.
5. The cut on the minimal energy deposit in the BPC was moved from 20 GeV to 18 GeV and 22 GeV.
6. The BPC fiducial area has been changed to :

   $$[5.37 \text{ cm} < X < 9.17 \text{ cm}] \text{ AND } [\ -2.22 \text{ cm} < Y < 2.58 \text{ cm}\ ]$$

7. The range of the invariant mass M_{KK} in which the Φ events were counted was changed from 1.0 GeV$< M_{KK} <$1.04 GeV to 0.99 GeV$< M_{KK} <$1.05 and 1.01 GeV$< M_{KK} <$1.03.
8. The different methods of determination of Φ events have been used (Sec. 5.4).
9. The uncertainty of the proton dissociation background in the final sample was assumed $\pm 7.5\%$ [16].

10. The uncertainty on the integrated luminosity is 3%.

The resulting systematic errors are listed in Tab 6.1.

Systematical check	Uncertainty %
$p_t(1,2)$ >100 MeV	±0.0
$p_t(1,2)$ >200 MeV	+2.6
$\|\eta(1,2)\|$ <1.5	-0.1
$\|\eta(1,2)\|$ <2.0	-0.3
$\|Z_{vtx}\|$ <40 cm	+0.2
$\|Z_{vtx}\|$ <60 cm	+0.1
E_{BPC} >18 GeV	+1.1
E_{BPC} >22 GeV	+1.5
6	+4.1
7	-3.2 / +1.4
8	-3.0 / +1.0
9	±7.5
10	±3.0
Added in quadrature	-9.0 / +10.0

Table 6.1: *List of sources of systematic errors.*

6.2 Cross section for the entire data sample

The cross sections were calculated according to Eq. 5.3 and 5.10, using the method presented in Sec. 5.3. The total cross section was quoted at values Q_0^2 and W_0, shown in the following table.

Range	$< Q^2 >$	Q_0^2	$< W >$	W_0
0.25 GeV^2 < Q^2 < 0.85 GeV^2 25.0 GeV< W < 90.0 GeV t< 0.6 GeV^2	0.46	0.55	51.6	57.5

The contribution to the final sample from events from the proton dissociation was assumed to be $C_{diss} = 24\%$ (Sec. 4.3.2) and the branching ratio for the $\Phi \to K^+K^-$decay was taken B=0.49 [52]. The integrated luminosity corresponding to the analysed data sample was L_{int}=9.79 pb^{-1} (Sec. 4.2). The same values for C_{diss}, B and L were used in determination of cross sections in W and Q^2 bins (following sections). The acceptance in the range : 0.25 GeV^2 < Q^2 < 0.85 GeV^2, 25.0 GeV< W < 90.0 GeV, t< 0.6 GeV^2 was determined to be $A_{tot} = 0.0312 \pm 0.0008$ (Sec. 5.2). The $\gamma^* p$ cross section in the above kinematical range, determined with method I, at $Q_0^2 = 0.55$ GeV$^2, W_0 = 57.5$ GeV is :

$$\sigma_{\gamma^* p \to \phi p}=343.0 \pm 25.0(stat.)^{+34}_{-32}(syst.) \text{ nb.}$$

As a cross check, the total cross section was also evaluated using four other methods

(Sec. 5.4) to determine numbers of Φ events and results are summarised in the Tab. 6.2. All values are consistent within the statistical errors.

N_Φ	$\sigma_{\gamma p\to\phi p}$[nb]	Comments
512.0±35.0	343.0±25.0	method I dE/dx eff. corr.
504.0±31.0	338.0± 23.0	method IIa fit before dE/dx, r=const
516.0±27.0	346.0±20.0	method IIb fit before dE/dx, r≠const
497.0±27.0	333.0±20.0	method IIc fit after dE/dx, r=const
504.0±27.0	338.0±20.0	method IId fit after dE/dx, r≠const

Table 6.2: *Total $\sigma_{\gamma^* p\to\phi p}$ cross sections using five methods of determining N_Φ (for details see Sec. 5.4).*

6.3 W dependence of the cross section

The cross section $\sigma_{\gamma^* p\to\phi p}$ was determined at three values of W_0 (Tab. 6.3), all extrapolated to $Q_0^2 = 0.55$ GeV^2. The number of events was determined using the particle identification method based on the energy loss dE/dx, corrected for the efficiency (method I) and alternatively from the fit to the M_{KK} distribution after dE/dx identification (method II). The results (method I) are summarised in Tab. 6.4. According to the Regge phenomenology, the W dependence of the cross section may be described by the exponential function $\sigma(W) \propto W^\alpha$. The fit yielded the value of $\alpha = 0.1 \pm 0.2$. The fitted function together with the data points is shown on Fig. 6.1. Within the large statistical errors the result is consistent with the value of $\alpha = 0.22$, predicted by Regge phenomenology.

W range [GeV]	$< Q^2 >$	$< W >$	W_0
25 - 40	0.46	32.4	32.5
40 - 60	0.45	50.5	50.0
60 - 90	0.47	75.3	75.0

Table 6.3: *Binning for the W dependence.*

W_0	N_Φ	A	$\sigma_{\gamma^* p\to\phi p}$[nb]
32.5	191.0 ± 21.0	0.032247	319.0 ± 38.0
50.0	176.0 ± 22.0	0.033	338.0 ± 45.0
75.0	147.0 ± 17.0	0.027737	349.0 ± 44.0

Table 6.4: $\sigma_{\gamma^* p\to\phi p}$ *as a function of W at $Q_0^2 = 0.55$ GeV^2.*

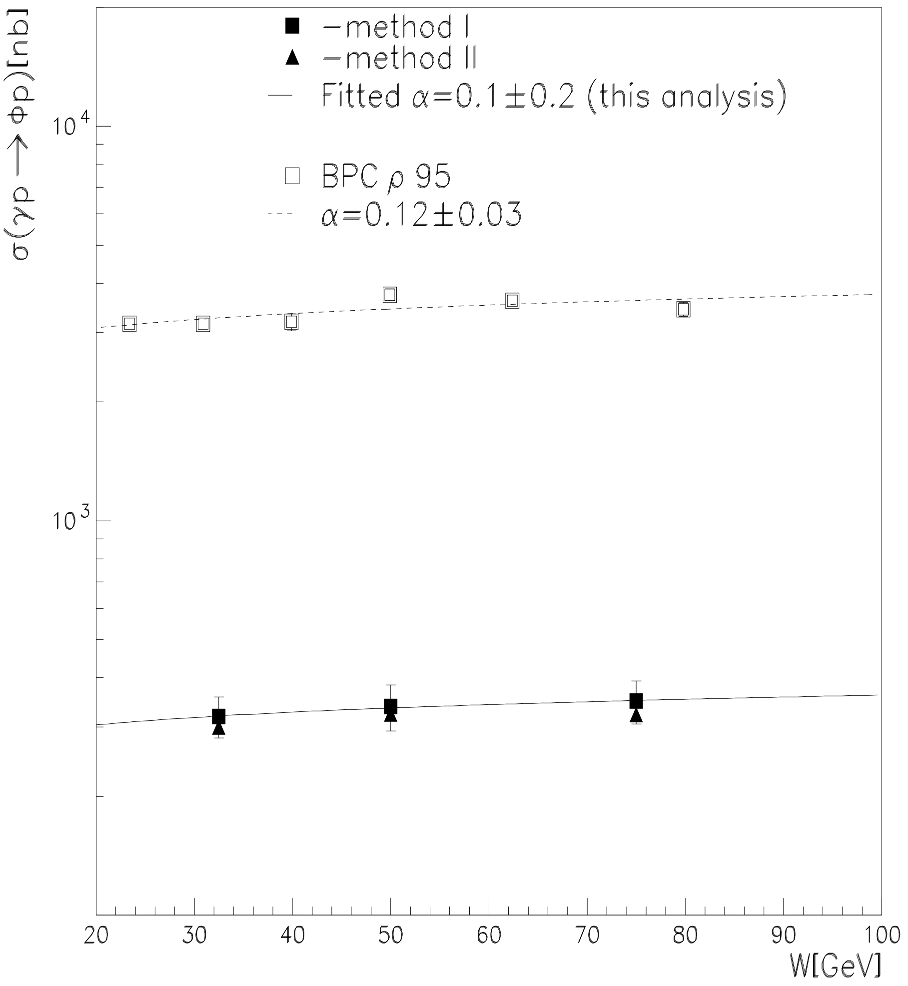

Figure 6.1: *W dependence of the cross section at $Q_0^2 = 0.55$ GeV^2. The curve shows the fit of the function $\sigma_{\gamma^* p \to \phi p}(W) \propto W^{\alpha}$.*

6.4 Q^2 dependence of the cross section

The $\sigma_{\gamma^* p \to \phi p}$ was measured at three values of Q_0^2 (Tab.6.5), all extrapolated to $W_0 = 57.5$ GeV. The number of Φ events was determined using the same two alternative methods as in case of W dependence (see above). Tab. 6.6 summarises the results (method I). The following parameterisation, motivated by the VMD model (Sec. 2.3.1), was fitted to the Q^2 dependence of the $\gamma^* p$ cross section:

$$\sigma(Q^2) \propto \frac{1}{(1 + Q^2/M_\Phi^2)^n} \; . \tag{6.1}$$

Q^2 range [GeV^2]	$< Q^2 >$	$< W >$	Q_0^2
0.25 - 0.4	0.31	50.7	0.325
0.4 - 0.6	0.49	53.4	0.5
0.6 - 0.9	0.72	55.2	0.75

Table 6.5: *Binning for the Q^2 dependence.*

Q_0^2	N_Φ	A	$\sigma_{\gamma^* p \to \phi p}$[nb]
0.325	207.0 ± 24.0	0.02723	458.0 ± 56.0
0.5	191.0 ± 20.0	0.03517	379.0 ± 43.0
0.725	113.0 ± 16.0	0.03225	284.0 ± 43.0

Table 6.6: *$\sigma_{\gamma^* p \to \phi p}$ as a function of Q^2 at $W_0 = 57.5$ GeV.*

The fit was performed using the experimental points from this analysis and ZEUS photoproduction [6] measurement. Because these results were obtained at different values of W, they were extrapolated to $W_1 = 70$ GeV according to the power-like behaviour, $\sigma(W) \propto W^\alpha$:

$$\sigma_{\gamma^* p \to \phi p}(Q_0^2, W_0 = 70.0) = \sigma_{\gamma^* p \to \phi p}(Q_0^2, W_1) \cdot \left(\frac{70}{W_1}\right)^\alpha . \tag{6.2}$$

The results of the present analysis were extrapolated using $\alpha = 0.22$. In Tab. 6.7 the results from photoproduction and DIS, before and after extrapolation are presented, together with the values of exponent α that were used in this procedure.

The fitted value of the exponent n in Q^2 dependence (Eq. 6.1) amounts to $n = 2.16 \pm 0.47$, the fitted curve is shown on Fig. 6.2. If the Eq. 6.1 is fitted to all data points from that figure, the value $n = 2.14 \pm 0.04$ is obtained.

6.5 Angular distributions.

The angular distributions of the decay kaons allow to determine certain Φ spin density matrix elements (Eq. 2.36). After integrating this formula over $\cos\theta_h$ or ψ_h, one dimensional distributions are obtained (Eq. 2.37 and 2.38). Fig. 6.3 shows the distribution of $\cos\theta_h$ and ψ_h for the entire data sample and Fig. 6.4 shows the distribution of $\cos\theta_h$ and ψ_h in two Q^2 bins. The matrix elements r_{00}^{04} and r_{1-1}^{1} can be determined by fitting these distributions with Eq. 2.37 and 2.38, respectively . The results of such fits are summarised in Tab. 6.8.

If SCHC holds then ratio of longitudinal and transverse cross section , R, is related to matrix element r_{00}^{04} (Eq. 2.39). The ratio R has been evaluated according to this equation and the results are presented in Tab. 6.9.

Q_0^2 [GeV^2]	W_0 [GeV]	$\sigma_{\gamma^* p \to \phi p}(W_0)$[nb]	$\sigma_{\gamma^* p \to \phi p}(W_1 = 70)$	α	Ref.
0.0	70	970.0± 190.0	970.0± 190.0	-	[6]
4.0	80	40.2± 3.1	37.34±2.9	0.56	[59]
7.0	80	14.5± 1.3	13.5±1.2	0.56	[59]
13.0	80	3.3± 0.6	2.9±0.5	0.9	[59]
8.2	94	10.3± 2.2	7.9±1.7	0.9	[15]
14.7	99	3.1± 0.7	2.3±0.5	0.9	[15]

Table 6.7: *Results from other exclusive Φ production measurements at ZEUS. α - the value of the power parameter used in the extrapolation procedure (Eq. 6.2).*

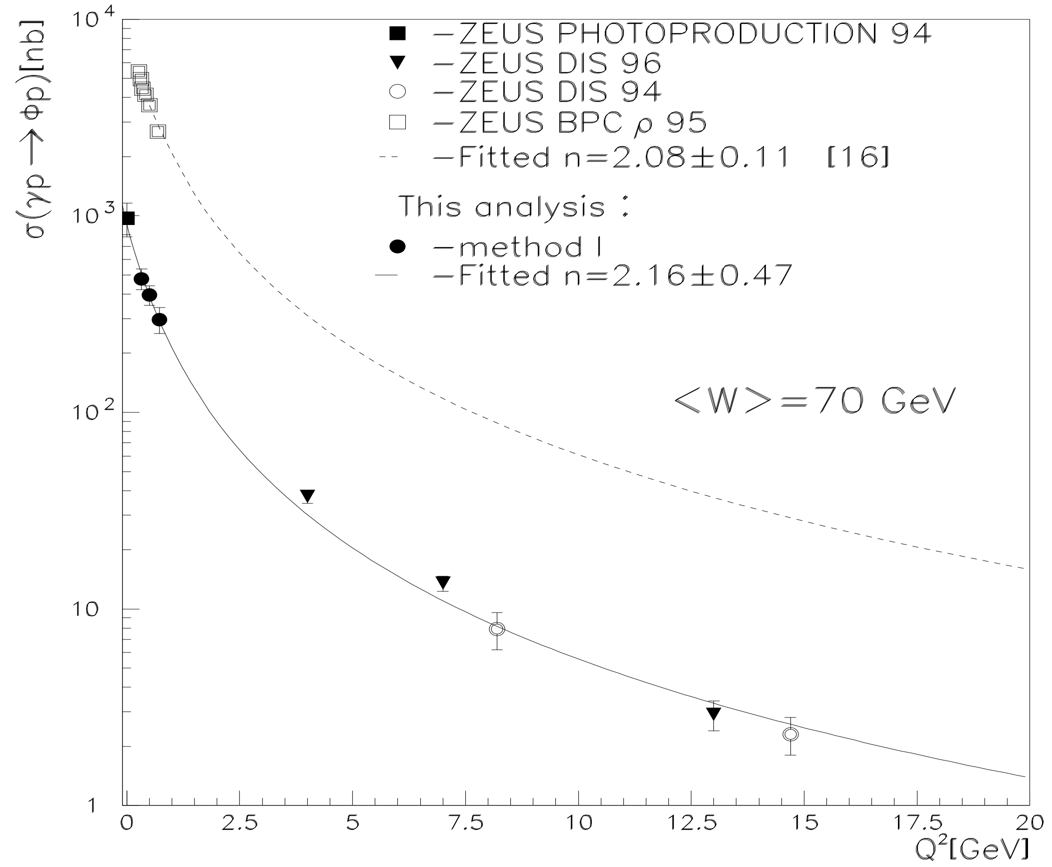

Figure 6.2: *Results on Q^2 dependence of the cross section at $W_0 = 57.5$ GeV. The curves show the fit of Eq. 6.1, dashed line is the dependence fitted in the ρ^0 analysis [16], solid line is the dependence fitted to experimental points from the present analysis and photoproduction [6].*

		This Analysis		BPC ρ^0 95	
Q^2 [GeV]^2 range	$< Q^2 >$ [GeV^2]	r_{00}^{04}	r_{1-1}^{1}	r_{00}^{04}	r_{1-1}^{1}
0.25-0.85	0.46	0.20 ±0.03	0.33 ± 0.03	0.26 ± 0.02	0.35 ± 0.01
0.25-0.45	0.34	0.18 ±0.05	0.29 ± 0.05	0.23 ± 0.01	0.36 ± 0.01
0.45-0.85	0.62	0.23 ± 0.05	0.37 ± 0.04	0.32 ± 0.01	0.31 ± 0.01

Table 6.8: *Values of matrix elements* r_{00}^{04} *and* r_{1-1}^{1} *obtained by fitting to angular distributions from Figs. 6.3 and 6.4, for* $< W >$*=51.6 GeV (this analysis); for comparison results for exclusive* ρ^0 *production in the same kinematical range are shown [16].*

$< Q^2 >$ [GeV^2]	This Analysis R	BPC ρ^0 95 R
0.46	0.25±0.05	0.35 ± 0.04 ± 0.04
0.34	0.22±0.07	0.30 ± 0.02 ± 0.03
0.62	0.30±0.08	0.47 ± 0.02 ± 0.04

Table 6.9: $R = \sigma_L/\sigma_T$ *ratio calculated from* r_{00}^{04} *using Eq. 2.39, for comparison results for exclusive* ρ^0 *production, calculated with the same method are shown [16].*

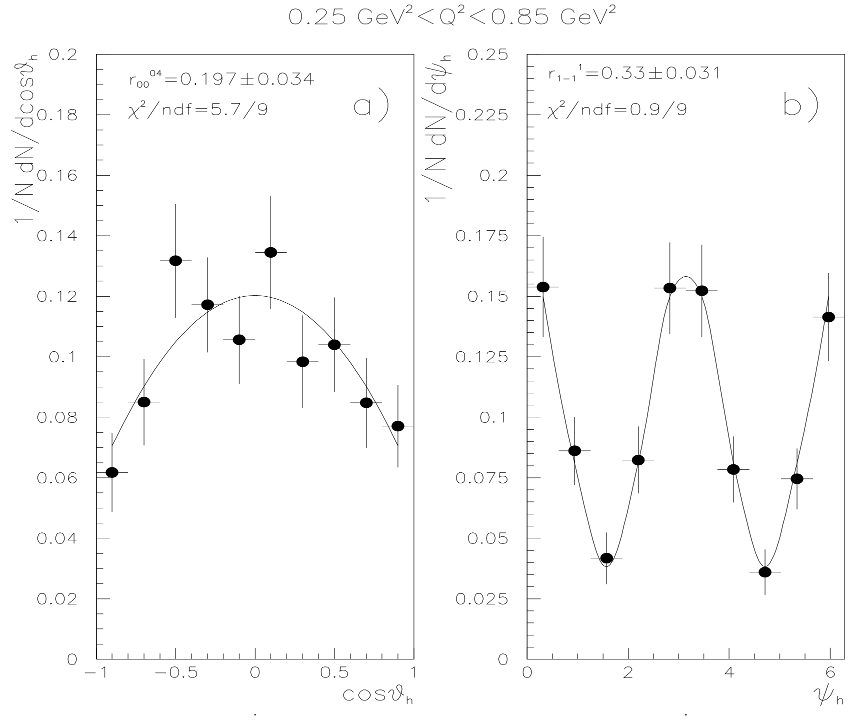

Figure 6.3: *Angular distributions for the entire sample : (a)* $\cos\theta_h$ *; (b)* ψ_h *.*

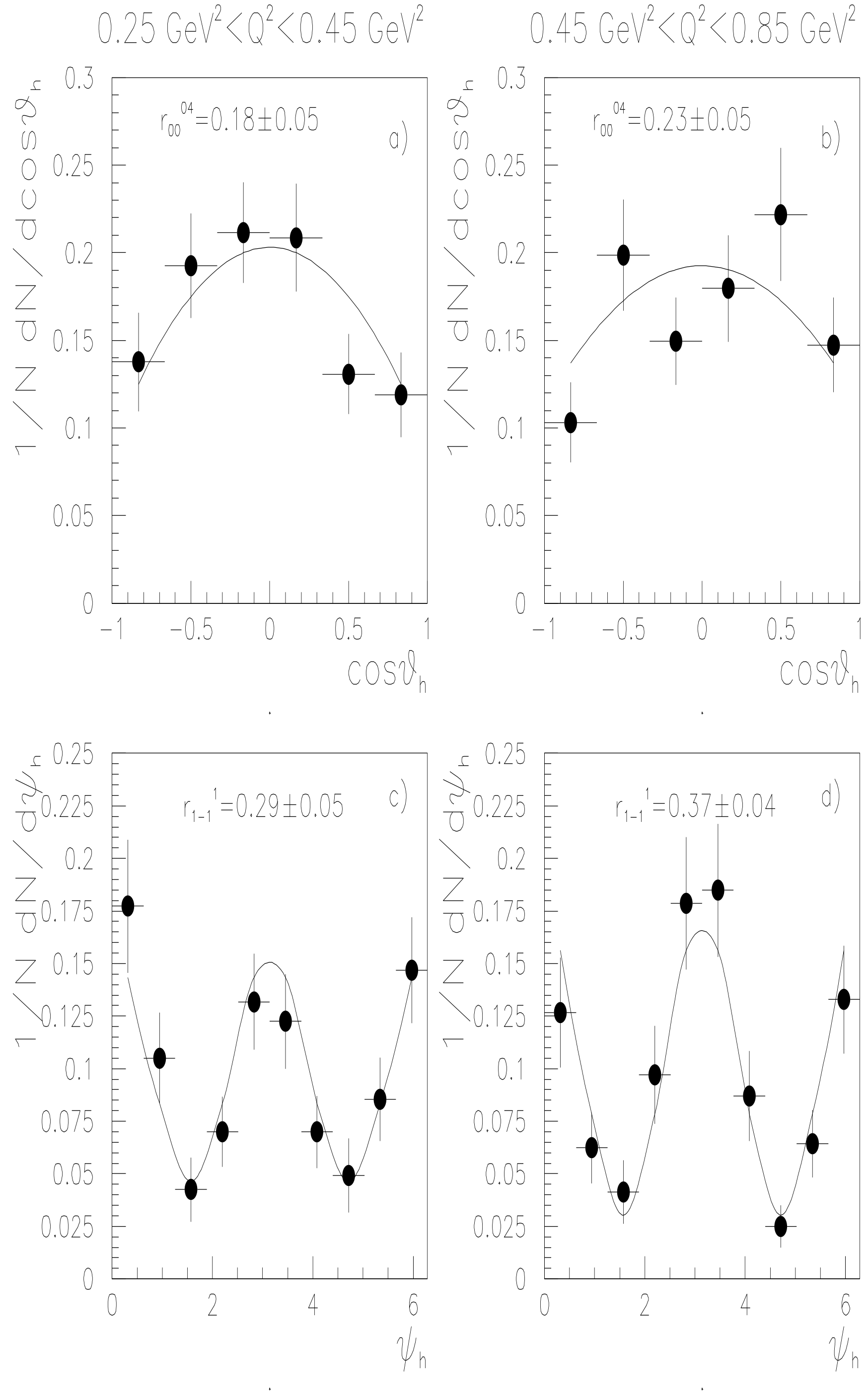

Figure 6.4: *Angular distributions for two intervals of* Q^2 *(a),(c) 0.25 GeV*^{2} $<Q^2<$ *0.45 and (b),(d) 0.45 GeV*^{2} $<Q^2<$ *0.85 .*

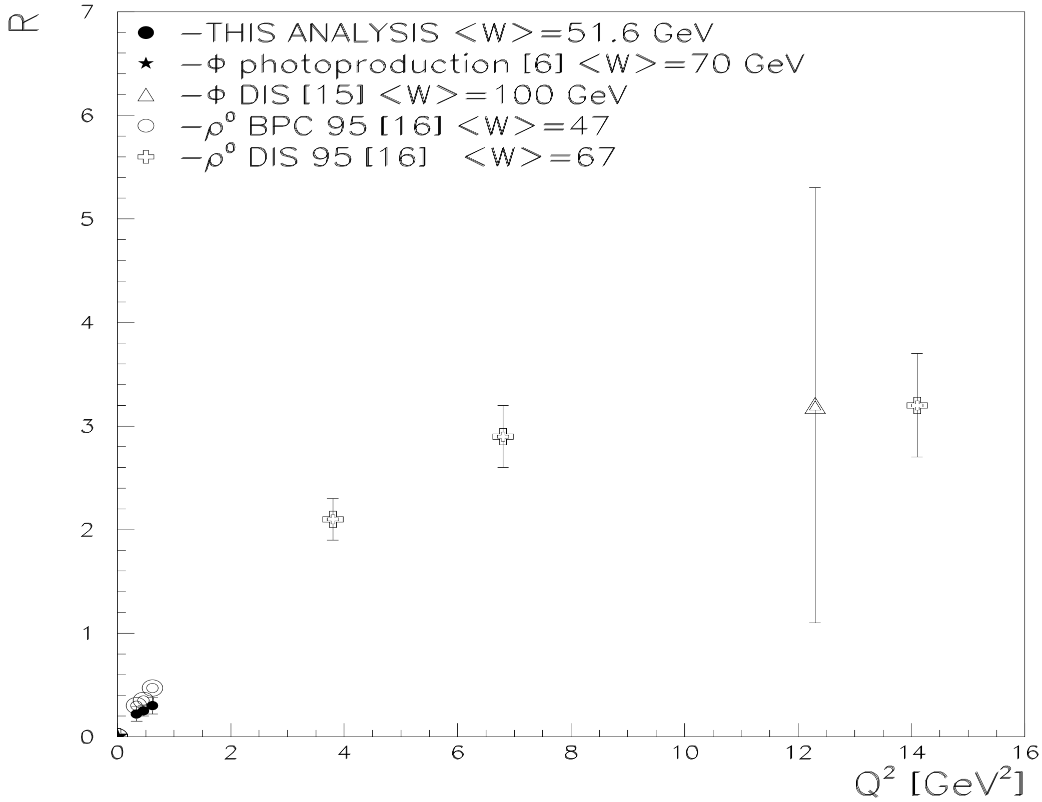

Figure 6.5: *The ZEUS results for $R = \sigma_L/\sigma_T$ ratio calculated from r^{04}_{00} using Eq. 2.39.*

Chapter 7

Summary and Conclusions

Properties of exclusive Φ production in the kinematical range : 25 GeV $< W <$ 90 GeV, 0.25 GeV ^{2} $< Q^2 <$ 0.85 GeV ^{2} and $|t| <$ 0.6 GeV^2 were studied using data collected with the ZEUS detector at the HERA collider. The integrated cross section in the above kinematical range is $\sigma_{\gamma^* p \to \phi p}$= 343.0 $\pm$25.0($stat.$) $^{+34}_{-32}$($syst.$) nb at W_0 = 57.5 GeV and Q^2_0=0.55 GeV^2.

The cross section was also determined in the three W and three Q^2 bins. The power like behaviour $\sigma(W) \propto W^\alpha$ was fitted at $Q^2_0 = 0.55$ GeV^2, yielding the value $\alpha = 0.1 \pm 0.2$. This value is consistent with $\alpha = 0.12 \pm 0.03$ measured in exclusive ρ^0 production in the same kinematical region [16]. Large statistical uncertainty of this result does not allow to make a precise conclusion on the energy dependence. Nevertheless the result, $\alpha = 0.1 \pm 0.2$, despite its large error, indicates that the hard regime ($\alpha \gtrsim 0.8$) does not manifest at these values of Q^2 in exclusive Φ production. Preliminary results of a corresponding measurement in DIS at $Q^2 = 5$ GeV^2, shown on Fig.8.1, indicate that the energy dependence may already be stronger than at low Q^2 : $\alpha = 0.56 \pm 0.18(stat.) \pm 0.19(syst.)$. A more abundant data is required to reach a definite conclusion on this subject. Comparison of measurements of exclusive Φ photoproduction and BPC Φ and ρ^0 suggest that these processes exhibit a comparable weak energy dependence, in contrast to a strong energy dependence for the J/ψ electroproduction ($\alpha \simeq 0.8$).

The Q^2 dependence of the cross section was also investigated. The parameterisation motivated by the VMD model (Eq. 6.1) has been fitted to the experimental points from this measurement and photoproduction [6], the fit yielded the value of the exponent $n = 2.16 \pm 0.47$. The fit was also performed to the experimental points from this measurement as well as photoproduction [6] and DIS [59, 15], yielding a consistent value $n = 2.14 \pm 0.04$. The value obtained for the BPC ρ^0 data is 2.08 ± 0.11 [16].

The Φ spin density matrix elements r^{04}_{00} and r^{1}_{1-1} were extracted from angular distributions. Assuming SCHC, the ratio of the longitudinal and transverse cross sections, R, was determined (Eq. 2.39) to be R=0.25 $\pm$ 0.05, for the entire sample. It was also

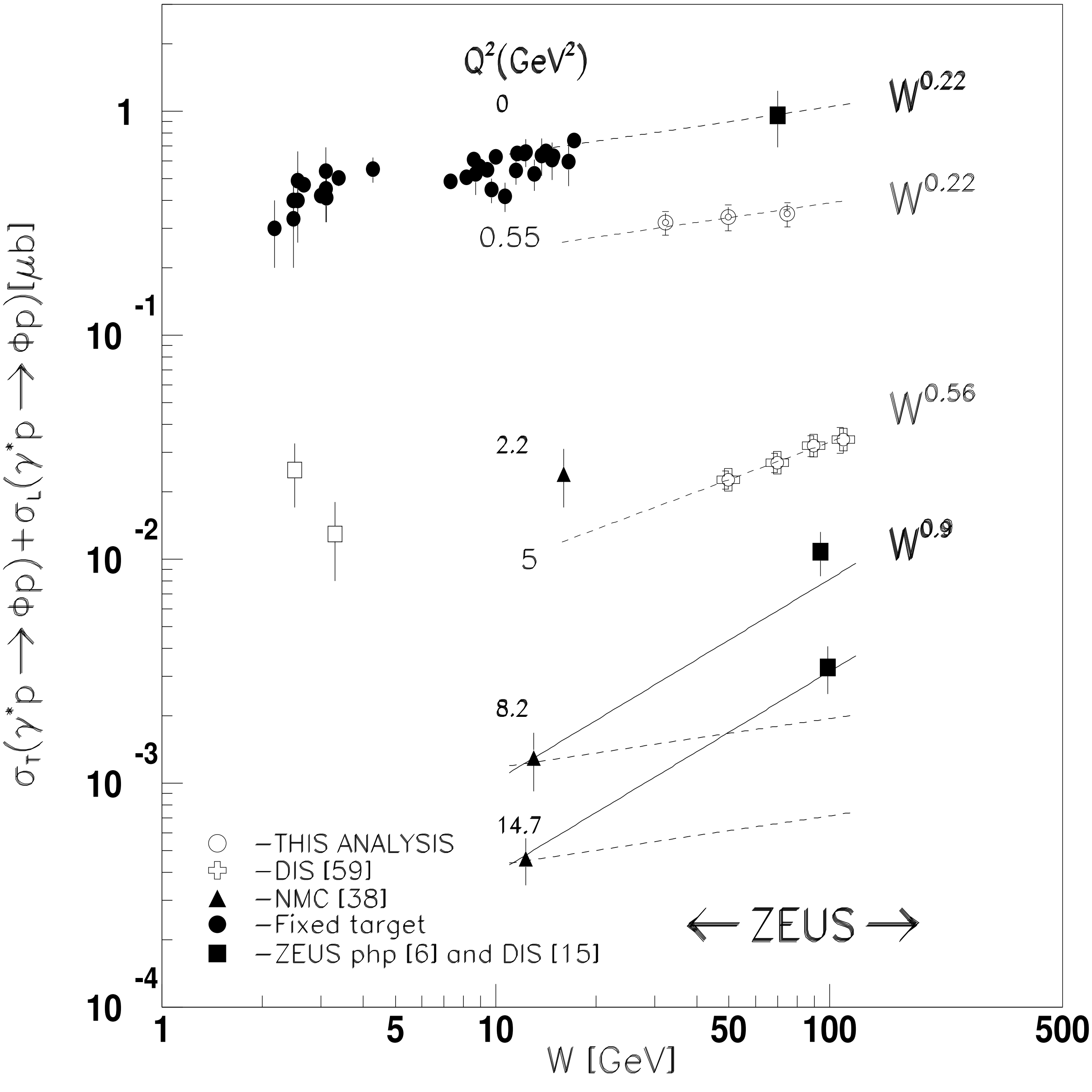

Figure 8.1: Cross section for Φ meson electroproduction measured in fixed target experiments and HERA experiments ZEUS and H1.

determined in two Q^2 intervals (Tab. 6.9). The ratio R from the present analysis is systematically smaller than the one measured in the BPC ρ^0 (Tab. 6.9) analysis but in view of statistical and systematic uncertainties no significant discrepancy is manifested. Both results indicate a rapid increase of R in the low Q^2 region, from $R = 0$ in photoproduction to $R \simeq 0.3 - 0.5$ at $Q^2 = 0.6$ GeV^2.

The particle identification based on energy loss dE/dx has been used, it enabled to significantly reduce the background contribution in the final data sample. The efficiency of this method of rejecting background events has been determined, according to which a novel method of determining number of Φ events has been used. The dE/dx can be a useful tool for particle identification in the ZEUS detector.

The present analysis and results can be also viewed as motivation for the effort to analyse the 1997 data, almost 3 times more abundant, in the nearest future - both at low Q^2 (BPC) and high Q^2 (DIS).

Acknowledgements

First of all I would like to thank my supervisor, Jacek Ciborowski for suggestions, comments and good atmosphere which were priceless for creation of this thesis. I wish to thank Krzysztof Muchorowski who was helpful in introducing me into the subject. Prof. Halina Abramowicz was always patient enough to indicate mistakes and suggest better solutions. I would like to thank Marcus Groll and Teresa Monteiro for numerous discussions. I would like also to thank the DESY Directorate for the financial support during my stay at DESY.

Bibliography

[1] T.H.Bauer et al.,Rev. Mod. Phys. 50 (1978) 261.

[2] J.Busenitz et al., Phys. Rev. D40 (1989) 1.

[3] R.M.Egloff et al., Phys. Rev. Lett. 43 (1979) 657.

[4] R.M.Egloff et al., Phys. Rev. Lett. 43 (1979) 1545.

[5] D.Westphal, 'Measurement of elastic ρ^0 Photoproduction at HERA', Ph.D. thesis., Univ. of Hamburg (1997).

[6] The ZEUS Collaboration,Measurement of Elastic ϕ Photoproduction at HERA, Phys. Lett. **B 377** (1996) 259.

[7] J.Grosse-Knetter, Measurement of Elastic ω Photoproduction at HERA, DESY F35D-97-02, University of Hamburg, Ph.D thesis, 1997.

[8] P.D.B Collins, An Introduction to Regge Theory and High Energy Physics (Cambridge University Press, 1977).

[9] J.J. Sakurai, Ann. Phys. 11 (1960) 1.

[10] ZEUS Collaboration, M.Derrick et al., Measurement of the Cross Section for reaction $\gamma p \to J/\psi p$, Phys. Lett. B350 (1995) 120.

[11] H1 Collaboration, S.Ahmed et al., Elastic and Inelastic Photoproduction of J/ψ at HERA, Nucl. Phys.,B472 (1996) 3.

[12] ZEUS Collaboration, J.Breitweg et al., Measurement of the Elastic J/ψ Photoproduction at HERA,Z. Phys. C75 (1997) 215.

[13] H.Beier, 'Diffractive Production of ρ^0 Mesons in Deep Inelastic Scattering at HERA', Ph.D. thesis., Univ. of Hamburg (1997).

[14] K.Muchorowski, 'Analysis of exclusive ρ^0 production in deep inelastic *ep* scattering at 300 GeV centre-of-mass energy (experiment ZEUS at HERA accelerator), Ph.D. thesis., Univ. of Warsaw (1998).

[15] The ZEUS Collaboration, Measurement of the Reaction $\gamma^* p \to \phi p$ in Deep Inelastic Scattering at HERA, Phys. Lett. B 380 (1996) 220.

[16] The ZEUS Collaboration, Exclusive Electroproduction of ρ^0 and J/ψ Mesons at HERA, to be published.

[17] M.G.Ryskin, Z. Phys. C57(1993)89;
M.G.Ryskin, et al.. hep-ph/9511228.

[18] S.J.Brodsky et al.,Phys. Rev. D50 (1994) 3134.

[19] J.J. Sakurai, Phys. Rev. Lett. 22 (1969) 981.

[20] A. Donnachie, P. V. Landshoff, Phys. Lett., B 185 (1987) 403, Nucl. Phys. B 311 (1989) 509.

[21] A. Donnachie, P. V. Landshoff, Phys. Lett., B 348 (1995) 213.

[22] A. Donnachie, P. V. Landshoff, Phys. Lett., B 296 (1992) 227.

[23] M.Derrick et al., Measurement of Elastic Omega Photoproduction at HERA, Z. Phys. C73 (1996) 73.

[24] H1 Collab., T.Ahmed et al., Phys. Lett. B299 (1993) 374.

[25] ZEUS Collab.,M.Derrick et al., Measurement of Total and Partial Photon Proton Cross Sections at 180 GeV Center of Mass Energy, Z. Phys. C63 (1994) 391.

[26] H1 Collab., T.Ahmed et al., Measurement of the Total Photon Proton Cross section and its Decomposition at 200 GeV Centre of Mass Energy DESY 95-162.

[27] The ZEUS Collaboration, Elastic and Proton-Dissociative ρ^0 Photoproduction at HERA, DESY 97-237.

[28] The ZEUS Collaboration, M.Derrick et al.,Phys. Lett. B356 (1995) 601.

[29] M.Binklay et al., Phys. Rev. Lett.48 (1982) 73.

[30] B.H.Denby et al., Phys. Rev. Lett.52 (1984) 795.

[31] T.Monteiro, private communications.

[32] T.Monteiro in Proceedings of the Workshop on Deep Inelastic Scattering and QCD (DIS97),edited by J.Repond (AIP, Chicago, 1997).

[33] T.Monteiro,'Exclusive electroproduction of ρ^0 mesons for $0.25 < Q^2 < 0.85$ GeV^2 at HERA',Ph.D. thesis,Univ. of Hamburg, in preparation.

[34] B.Surrow 'Measurement of the Proton Structure Function F_2 at Low Q^2 and Very Low x with the ZEUS Beam Pipe Calorimeter at HERA', Ph.D. thesis., Univ. of Hamburg (1998).

[35] J.A. Crittenden et al., DESY 97-068 (1997).

[36] The H1 Collaboration, Proton Dissociative ρ and Elastic ϕ Electroproduction at HERA, DESY 97-082.

[37] The EMC Collaboration, Z. Phys. C 39 (1988) 169.

[38] The NMC Collaboration, Nucl.Phys. B 429 (1994) 503.

[39] F.Halzen and A.D.Martin, Quarks and Leptons, (John Wiley Sons Inc., New York, 1984).

[40] J.D.Jackson, Remarks on the Phenomenological Analysis of Resonances, Nuovo Cimento 34 (1964) 1644.

[41] K.Schilling and G.Wolf, How to Analyse Vector-Meson Production in inelastic Lepton Scattering, Nucl. Phys. B61 (1973) 381.

[42] A. Levy, DESY 97-013 (1997)

[43] L.N.Hand, Phys. Lett. B 129 (1963) 1834.

[44] C.G.Callan and D.Gross,Phys. Rev. Lett. 22 (1969) 156.

[45] Ann. Phys 5, 325; Z Phys. 81, 363

[46] R.Brun et al., MINUIT Reference Manual, CERN (1997).

[47] R.Brun et al., PAW Reference Manual,, CERN (1997).

[48] R.Brun et al., HBOOK Reference Manual, CERN (1997).

[49] ZEUS student seminar, 'Particle Identification using the dE/dx of the CTD', 22 Apr 97.

[50] O.Deppe, private communication.

[51] O.Deppe, Measurement of the Charm Part of the Proton Structure Function F_2 at HERA. PhD thesis, Univ. Hamburg, 1998, in preparation.

[52] Particle Data Group, R.M.Barnett et al.,Phys. Rev. D 54 (1996) 1.

[53] The ZEUS Collaboration, M.Derrick et al., Status Report 1993,DESY (1993).

[54] S.Bentvelsen et al., Physics at HERA Proceedings, Hamburg 1991,ed. by W.Buchmuller and G.Ingelman.

[55] G.F.Hartner et al., ZEUS-Note 97-064, internal report.

[56] The ZEUS Collaboration, N-639, XXIX International Conference on High Energy Physics, Jerusalem 19-26 August 1997.

[57] The H1 Collaboration, 381, XXIX International Conference on High Energy Physics, Jerusalem 19-26 August 1997.

[58] A. Proskuryakov, private communication.

[59] S. Kananov, 6-th International Workshop on Deep Inelastic Scattering and QCD, 4-8 April 1998, Brussels .

[60] M. Arneodo, L.Lamberti and M.G. Ryskin, Comp. Phys. Comm. 100 (1997) 195.

[61] H.Bethe and W.Heitler, Proc. Roy. Soc. A146(1934)83.